Electrical Double Layers: Effects of Asymmetry in Electrolyte Valence on Steric Effects, Dielectric Decrement and Ion-Ion Correlations

Ankur Gupta and Howard A. Stone*

Department of Mechanical and Aerospace Engineering, Princeton University, Princeton, NJ 08544

E-mail: hastone@princeton.edu

Abstract

We study the effects of asymmetry in electrolyte valence (i.e. non $z:z$ electrolytes) on mean field theory of the electrical double layer. Specifically, we study the effect of valence asymmetry on finite ion-size effects, the dielectric decrement and ion-ion correlations. For a model configuration of an electrolyte near a charged surface in equilibrium, we present comprehensive analytical and numerical results for the potential distribution, electrode charge density, capacitance, and dimensionless salt uptake. We emphasize that the asymmetry in electrolyte valence significantly influences the diffuse-charge relations and prior results reported in the literature are readily extended to non $z:z$ electrolytes. We develop scaling relations and invoke physical arguments to examine the importance of asymmetry in electrolyte valence on the aforementioned effects. We conclude by providing implications of our findings on diffuse-charge dynamics and other electrokinetic phenomena.

Keywords: Diffuse-charge, Capacitance, Debye length, Finite ion size, Poisson-Boltzmann

Introduction

Diffuse charge refers to the distribution of ions in an electrolyte solution adjacent to a charged solid surface. The charge profile is critical to a variety of applications; in colloid science and microfluidic applications, diffuse charge is important in electrophoresis,[1–3] electroosmosis,[1–5] and diffusiophoresis,[6,7] while in energy storage devices, the charged layers form the basis of electrochemical capacitors,[8,9] and more recently semi-solid flow capacitors.[10] The properties of diffuse charge are typically determined by the widely used Gouy-Chapman (GC) theory, which describes the dependence of surface charge density q and capacitance $\mathbb{c}$ on the potential drop ψ_D across the diffuse-charged region.[11–16]

The classical GC results are based on a mean-field approximation and provide analytical expressions for $q(\psi_D)$ and $\mathbb{c}(\psi_D)$. Due to their relatively simple nature, GC results continue to be widely used, even though it is well recognized that they suffer from several limitations.[17–23] To improve the predictions of the GC results, several modifications have been suggested in the literature while retaining the mean-field framework of the classical GC results. In this article, we focus on three such modifications for valence asymmetric (or non $z:z$) electrolytes: finite ion-size effects, dielectric decrement and ion-ion correlations, and we indicate below earlier work in each area.

We first discuss finite ion-size effects, also commonly known as steric effects. The classical GC results are obtained by solving the Poisson-Boltzmann equations where ions are treated as point charges. Therefore, the classical GC results predict an unphysical outcome that ion concentration can increase indefinitely with increase in $|\psi_D|$. This limitation was recognized already 90 years ago by Stern,[17] Bikerman[18] and Freise,[19] and these authors accounted for the finite-ion size effects by assuming a simple hard-sphere model with a finite diameter of ions. A vast literature is available in this area and we only discuss a few reports in detail. For a more in-depth review of the literature on finite-ion size effects, including

more sophisticated models for spherical ions, we refer the readers to references 20, 21, 24–26. For example, Borukhov *et al.*[27] derived an expression for the concentration of ions with a finite ion size for a valence symmetric (or $z:z$), as well as valence asymmetric, or non $z:z$ electrolyte near a charged substrate. Kilic *et al.*[21,28] and Kornyshev[20] derived the modified Poisson-Boltzmann equations, and provided explicit expressions for $q(\psi_D)$ and $\mathbb{c}(\psi_D)$ for $z:z$ electrolytes while assuming that the cation and anion diameters are equal. In these articles, the authors also discussed the implications of including steric effects on the dynamics of diffuse charge. More recently, Han *et al.*[29] derived the results for $q(\psi_D)$ and $\mathbb{c}(\psi_D)$ for $z:z$ electrolytes but allowed the cation and anion diameters to be unequal, thus extending the results of Kilic *et al.*[21,28] and Kornyshev.[20] We emphasize that equality of cation and anion valence is a common assumption. In this article, we relax this assumption and we further extend the above mentioned results to non $z:z$ electrolytes. We show that asymmetry in cation and anion valence significantly influences the behavior of $q(\psi_D)$ and $\mathbb{c}(\psi_D)$.

Second, we focus on the effect of the dielectric decrement, which refers to the decrease in the dielectric constant due to a reduction in the orientational polarizability of the hydrated ions with increase in electrolyte concentration. A decrease in the dielectric constant lowers the ability to store charge in the double layer. The dielectric decrement is a well-known effect and has been recognized in several reports.[18,22,26,30–34] Here, we focus on the recent results of Nakayama and Andelman,[32] which describe the interplay between finite ion-size effects (with equal cation and anion diameters) and the dielectric decrement for $z:z$ electrolytes. In particular, we derive general results for the dielectric decrement for non $z:z$ electrolytes while also allowing for unequal cation and anion diameters. We then focus on the effect of valence asymmetry and show that it strongly impacts the double layer properties.

The ion-ion correlation effect, also known as the overscreening effect, relates to the interaction between nearby ions. This effect can be accounted for in the mean-field framework by

defining a screening length and including an additional fourth-order term in the modified Poisson-Boltzmann equations, as recently derived by Bazant, Storey and Kornyshev,[23,35] who discussed the competition between steric effects and ion-ion correlations. The authors showed that ion-ion correlations give rise to oscillations in charge density profiles, especially for large screening lengths.[23,35] We note that the article by Bazant and Storey[35] considers $1:1$ and $1:2$ electrolytes with equal cation and anion diameters. In this article, we extend these results for non $z:z$ electrolytes with different cation and anion diameters, and investigate the effect of electrolyte valence on ion-ion correlations.

Before proceeeding further, we acknowledge that we are certainly not the first to investigate non $z:z$ electrolytes. The effect of electrolyte valence has been investigated for the classical Poisson-Boltzmann equations,[11,36–42] e.g., Gouy,[11] Levine and Jones[37] and Grahame[36] analyzed the scenarios of $z_-/z_+ = 2$ or $z_-/z_+ = 1/2$. On the other hand, Lyklema[38] and Levie[40] described $\mathbb{c}(\psi_D)$ for a general combination of z_+ and z_-, though the results are presented in an awkward dimensional form. However, the equilibrium relationships for non $z:z$ electrolytes in the modified Poisson-Boltzmann description are not readily available. Therefore the aim of this article is to investigate the impacts of asymmetry in electrolyte valence on the modified Poisson-Boltzmann equations. We find that inclusion of asymmetry in electrolyte valence is critical as it affects all of the effects mentioned above.

We present some physical arguments to broadly highlight the importance of asymmetry in electrolyte valence. Since the magnitude of valence dictates the force experienced by the ions, when cations and anions are of different valence, the magnitude of forces experienced by the cations and anions are unequal, which creates an asymmetry in double layer properties, or $q(\psi_D) \neq q(-\psi_D)$ and $\mathbb{c}(\psi_D) \neq \mathbb{c}(-\psi_D)$. This apparent breaking of symmetry can have significant implications. For instance, several experimental data sets published in the supercapacitor literature utilize valence asymmetric electrolytes such as Na_2SO_4 and $CaCl_2$.[43,44]

However, the modeling approaches in this area are still typically restricted to $z:z$ electrolytes,[45] and thus studies have not been conducted to exploit valence asymmetry as a way to tune the energy and power density of supercapacitors. Similarly, valence asymmetry can be important for capacitive deionization,[3,46] a process where toxic ions migrate move from the bulk to the double layer. Here, capacitance would influence the quantity of toxic ions depleted as well as the time required for the depletion.[3] Since $\mathbb{c}(\psi_D) \neq \mathbb{c}(-\psi_D)$ for valence asymmetric ions, the direction of the potential drop will impact the efficacy of the process.

We also emphasize that our analysis is general since we consider a combination of valence asymmetry with other effects, *i.e.* finite ion sizes, dielectric decrement and ion-ion correlations. To highlight the relative importance of simultaneous effects, we now present a physical argument for the scenario where the combined effects of valence asymmetry and finite ion sizes are relevant. Let us assume that in an electrolyte, anions have a higher valence than the cations. At the same time, the anions have a significantly smaller ion size than the cation. When such an electrolytes comes in contact with a positively charged surface, the anions migrate towards the charged surface and cations move away from the surface. The higher valence of the anions leads to a rapid increase in the anion concentration with increase in ψ_D until there is no longer space to accommodate more anions. Therefore, a higher valence implies that the double layer saturates with anions at a smaller value of ψ_D. In contrast, the smaller anion size implies that each ion occupies a smaller volume, and thus saturation of double with anions occurs at a larger values of ψ_D. Therefore, valence asymmetry can either compete or cooperate with other additional effects, and thus provides flexibility in design of processes where the additional effects are significant.

In this article, we study the influence of asymmetry in electrolyte valence on finite ion-size effects (with unequal cation and anion diameters), dielectric decrement and ion-ion correlations. For each of these effects, we first derive the diffuse-charge relations for a general

valence electrolyte and provide analytical and numerical results for the potential distribution, $q(\psi_D)$, $\mathbb{c}(\psi_D)$ and dimensionless salt uptake $\alpha(\psi_D)$. Under appropriate assumptions, we recover previously reported results for $q(\psi_D)$ and $\mathbb{c}(\psi_D)$, thus highlighting the generality of the proposed relations. Since $\mathbb{c}(\psi_D)$ has multiple local extrema, we provide scaling relations to better explain the dependence of the extrema on different parameters. Lastly, we discuss the implications of our results on diffuse-charge dynamics and dimensionless parameters that govern the electrokinetic phenomena. We conclude by providing limitations of the models and directions for future research.

Problem setup

We consider an electrolyte in equilibrium with a charged surface (Fig. 1). Due to electrostatic attraction, oppositely-charged ions (also referred as counter ions) migrate towards the charged surface, and compete with thermal or entropic effects to create a region of diffuse charge. The typical thickness of the region of excess charge, or double layer, is given by the Debye length λ_D [15,16,38,47]

$$\lambda_D = \sqrt{\frac{\varepsilon_0 \varepsilon_s k_B T}{e^2 \sum_i z_i^2 c_{0,i}}}, \tag{1}$$

where ε_0 is the electrical permittivity of vacuum, ε_s is the dielectric constant of the solution without the electrolyte, k_B is the Boltzmann constant, T is temperature, z_i is the valence of the i^{th} ion type, $c_{0,i}$ is the bulk concentration of the i^{th} ion type, and e is the charge on an electron. The sum is over all ionic species present in the solution. The region close to the electrode where ions are adsorbed at the surface is known as the Stern layer (Fig. 1). The (molecular) thickness of the Stern layer is denoted λ_S.

To be specific, we consider an electrolyte with one cation type and one anion type. The cation and anion valences are denoted z_+ and z_- respectively. Since the electrolyte in bulk is neutral, the ion concentrations in bulk are $c_+ = z_- c_0$ and $c_- = z_+ c_0$. For instance, K_2SO_4

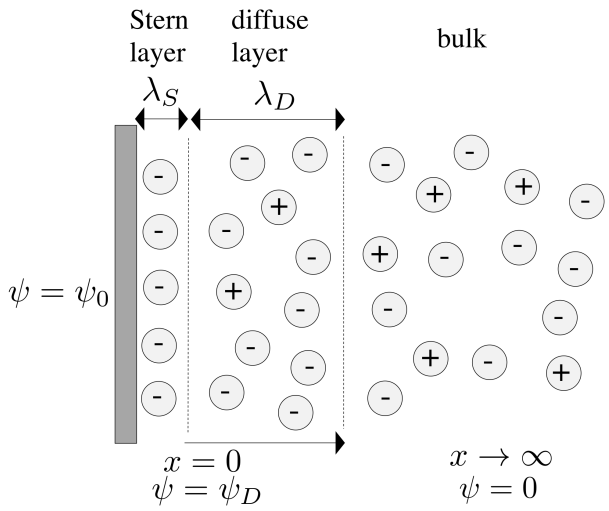

Figure 1: An electrolyte with cation valence z_+ and anion valence z_- is near a charged surface. The Stern layer thickness is denoted λ_S and the Debye length is denoted λ_D. The potential at the electrode is taken as $\psi = \psi_0$, the potential at the boundary between the Stern layer and diffuse layer is $\psi = \psi_D$, and the potential in bulk is zero.

is denoted by $z_+ = 1$, $z_- = 2$, $c_+ = 2c_0$, and $c_- = c_0$. Therefore, for a $z_+ : z_-$ electrolyte, according to Equation (1), λ_D is given as

$$\lambda_D = \sqrt{\frac{\varepsilon_0 \varepsilon_s k_B T}{z_+ z_- (z_- + z_+) e^2 c_0}}. \tag{2}$$

Finite ion-size effects

In this section, we consider finite ion-size effects and specifically focus on the effect of valence asymmetry on double layer properties. For simplicity, we assume that the relative permittivity ε is independent of $c_\pm$, or $\varepsilon(c_\pm) = \varepsilon_s$. However, we discuss the effect of a change in dielectric constant $\varepsilon(c_\pm)$ separately in the next section. Similarly, we also exclude the ion-ion correlations in this section but discuss their effect in the subsequent section.

Derivation

Potential distribution and charge accumulated

To include the finite ion-size effects, we assume a hard-sphere model where ions are spherical and are described with an effective diameter. Depending on the interaction between different ion types, the effective diameter may or may not be the same as the ion diameter. We refer the readers to references 20, 21, 28 for a more detailed discussion on effective diameters and the length scale of interactions. Here, we denote the effective diameter of a cation is a_+. Typically, $a_+ = \mathcal{O}(10^{-1} - 10)$ nm, and thus the concentration of cations cannot exceed $\frac{1}{a_+^3} = \mathcal{O}(10^{24} - 10^{30})$ m^{-3}.[21] We also allow for asymmetry in the effective diameter of anions and cations, and define the effective diameter of an anion as a_-. Therefore, the concentration of anions cannot exceed $\frac{1}{a_-^3}$.

The free energy of the system per unit volume F is defined as

$$F = U - TS, \tag{3}$$

where U is the internal energy per unit volume, S is the entropy per unit volume, and $F(\psi, c_\pm)$. U is defined as[20,21,32]

$$U = -\frac{\varepsilon_0 \varepsilon_s}{2} \left| \frac{d\psi}{dx} \right|^2 + z_+ e c_+ \psi - z_- e c_- \psi, \tag{4}$$

where $\psi(x)$ is the potential at a location x relative to a reference potential at $x \to \infty$, or $\psi(\infty) = 0$. The first term in Equation (4) represents the energy stored in the electric field and the remaining two terms account for the potential energy of the ions. To evaluate S, we use Boltzmann's formula to evaluate entropy of mixing $S = k_B \ln \omega$, where ω is the number of microstates. To estimate ω, we first estimate the number of ways to arrange the larger ions and then multiply with the number of ways to arrange the smaller ions. Here,

for convenience, we assume that $a_+ \geq a_-$. We estimate entropy as

$$-\frac{S}{k_B} = c_+ \ln\left(a_+^3 c_+\right) + \frac{1 - a_+^3 c_+}{a_+^3} \ln\left(1 - a_+^3 c_+\right) + c_- \ln\left(\frac{a_-^3 c_-}{1 - a_+^3 c_+}\right) + \frac{(1 - a_+^3 c_+ - a_-^3 c_-)}{a_-^3} \ln\left(\frac{1 - a_+^3 c_+ - a_-^3 c_-}{1 - a_+^3 c_+}\right). \tag{5}$$

An equivalent expression of entropy for $a_- \geq a_+$ can be estimated by switching the positive and negative subscripts. With $F(c_\pm)$ given by Equations (3) - (5), we evaluate the chemical potentials $\mu_\pm$ as

$$\mu_+ = \frac{\partial F}{\partial c_+} = z_+ e\psi + k_B T \left[\ln\left(\frac{a_+^3 c_+}{1 - a_+^3 c_+}\right) - \frac{a_+^3}{a_-^3} \ln\left(\frac{1 - a_+^3 c_+ - a_-^3 c_-}{1 - a_+^3 c_+}\right)\right], \tag{6a}$$

$$\mu_- = \frac{\partial F}{\partial c_-} = -z_- e\psi + k_B T \ln\left(\frac{a_-^3 c_-}{1 - a_+^3 c_+ - a_-^3 c_-}\right). \tag{6b}$$

We define dimensionless concentrations as $n_+ = \dfrac{c_+}{z_- c_0}$, $n_- = \dfrac{c_-}{z_+ c_0}$, and the dimensionless electric potential as $\Psi = \dfrac{e\psi}{k_B T}$. At equilibrium, the chemical potential is constant for all x, $\mu_\pm(x) = \mu_\pm(\infty)$, and we obtain

$$n_+ = \frac{\exp(-z_+ \Psi)}{g(\Psi)}, \tag{7a}$$

$$n_- = \frac{\exp(z_- \Psi) f(\Psi)}{g(\Psi)}, \tag{7b}$$

$$g(\Psi) = f(\Psi) + z_- a_+^3 c_0 \left(\exp(-z_+ \Psi) - f(\Psi)\right) + z_+ a_-^3 c_0 f(\Psi) \left(\exp(z_- \Psi) - 1\right), \tag{7c}$$

$$f(\Psi) = \left(1 + \frac{z_+ a_-^3 c_0 \left(\exp\left(z_- \Psi\right) - 1\right)}{1 - z_- a_+^3 c_0}\right)^{\frac{a_+^3}{a_-^3} - 1}. \tag{7d}$$

Physically, $g(\Psi)$ accounts for the reduction in concentration due to finite ion sizes and $f(\Psi)$ accounts for the change in concentration due to the contrast in ion sizes (note $f(\Psi) = 1$ for $a_- = a_+$). For $a_\pm \to 0$ in Equation (7), we recover the Boltzmann distribution. For $a_+ = a_-$ and $z_+ = z_-$, we recover the standard result in reference 21, 27, 28. Furthermore,

for $a_+ \neq a_-$ and $z_+ = z_-$, we recover the known result in reference.[29] To solve for $c_\pm$ and ψ, we couple Equation (7) with Gauss's law,

$$\varepsilon_0 \varepsilon_s \frac{d^2\psi}{dx^2} = e(z_- c_- - z_+ c_+). \tag{8}$$

which is to be solved with boundary conditions $\psi_0 = \psi(0) - \lambda_S \left.\frac{d\psi}{dx}\right|_{x=0}$ and $\psi(\infty) = 0$, where $\psi(0) = \psi_D$ is the potential drop across the diffuse layer (Fig. 1). We note that the boundary condition at the electrode assumes a thin Stern layer.[3] We non-dimensionalize with $\Psi = \frac{e\psi}{k_B T}$, $X = \frac{x}{\lambda_D}$, and $\Lambda_S = \frac{\lambda_S}{\lambda_D}$ to obtain

$$\frac{d^2\Psi}{dX^2} = \frac{n_- - n_+}{z_+ + z_-}, \tag{9}$$

with two boundary conditions

$$\Psi_0 = \Psi_D - \Lambda_S \left.\frac{d\Psi}{dX}\right|_{X=0}, \tag{10a}$$

$$\Psi(\infty) = 0. \tag{10b}$$

Equations (7) and (9) are governed by four dimensionless parameters: z_+, z_-, $a_+^3 c_0$, and a_+^3/a_-^3. To solve for Ψ and $n_\pm$, we assume z_+, z_-, $a_+^3 c_0$, a_+^3/a_-^3, Λ_S and Ψ_0 (the potential measured on the solid boundary) are specified. Typically, $a_\pm^3 c_0 = \mathcal{O}(10^{-10} - 10^{-1})$. For a more detailed discussion on the physical interpretation of $a_\pm^3 c_0$ and the range of possible values of $a_\pm^3 c_0$, we refer the reader to reference 21. We multiply both sides of Equation (9) by $\frac{d\Psi}{dX}$ and integrate once (using (10b)) to find

$$\frac{d\Psi}{dX} = -\mathrm{sgn}(\Psi)\sqrt{\frac{2}{z_+ z_- (z_+ + z_-) a_+^3 c_0} \ln g(\Psi)}, \tag{11}$$

where $\mathrm{sgn}(\Psi)$ is the sign function. For $a_+^3 c_0 \to 0$, $a_+/a_- = 1$, and $z_+ = z_- = z$, Equation (11) becomes $\frac{d\Psi}{dX} = -2\sinh\frac{z\Psi}{2}$, and another integration yields the well-known relation $\tanh\frac{z\Psi}{4} = \tanh\frac{z\Psi_D}{4}\exp(-X)$,[11] where Ψ_D is related to Ψ_0 through the boundary condition

in Equation (10a). For $a_+ \neq 0$, $a_+/a_- \neq 1$ and $z_+ \neq z_-$, we numerically integrate Equation (11) with the Stern layer boundary condition (10a) to obtain $\Psi(X)$, and the results are discussed later.

Next, we evaluate the surface charge density on the electrode as $q = -\varepsilon_0\varepsilon_s \left.\dfrac{d\psi}{dx}\right|_{x=0}$. Similarly, we can also calculate the capacitance $\mathfrak{c}$, *i.e.* the charged stored in the electrode per unit total potential drop, or $\mathfrak{c} = \left|\dfrac{dq}{d\psi_0}\right|$. It is convenient to non-dimensionalize $Q = \dfrac{q}{z_+ z_- (z_+ + z_-) e \lambda_D c_0}$ and $\mathbb{C} = \dfrac{\mathfrak{c}\lambda_D}{\varepsilon_0\varepsilon_s}$, such that $Q = -\left.\dfrac{d\Psi}{dX}\right|_{X=0}$ and $\mathbb{C} = \left|\dfrac{dQ}{d\Psi_0}\right|$. Thus, from Equation (11), we find the dimensionless surface charge density

$$Q = \mathrm{sgn}(\Psi_D)\sqrt{\frac{2}{z_+ z_- (z_+ + z_-) a_+^3 c_0} \ln g(\Psi_D)}. \tag{12}$$

Capacitance

To calculate $\mathbb{C} = \left|\dfrac{dQ}{d\Psi_0}\right|$, we write the Stern layer boundary condition in Equation (10a) as $\Psi_0 = \Psi_D + \Lambda_S Q$. Differentiating this relation with respect to Ψ_D, we get $\dfrac{d\Psi_0}{d\Psi_D} = 1 + \Lambda_S \dfrac{dQ}{d\Psi_D}$. Thus $\mathbb{C} = \left|\dfrac{dQ}{d\Psi_D}\dfrac{d\Psi_D}{d\Psi_0}\right|$, or

$$\mathbb{C}^{-1} = \left|\left(\frac{dQ}{d\Psi_D}\right)^{-1}\right| + \Lambda_S, \tag{13}$$

so that

$$\mathbb{C}^{-1} = \sqrt{\frac{2(z_+ + z_-)\ln g(\Psi_D)}{z_+ z_- a_+^3 c_0}} \frac{1}{|n_-(\Psi_D) - n_+(\Psi_D)|} + \Lambda_S. \tag{14}$$

Equations (13 - 14) demonstrate the well-known result that we can characterize the system as an electrical circuit with a capacitor representing the Stern layer and a capacitor representing the diffuse layer in series. For $a_+ \to 0$, $a_+/a_- = 1$, and $z_+ = z_- = z$, Equations (12) and

(14) take the form

$$Q = \frac{2}{z}\sinh\frac{z\Psi_D}{2}, \tag{15a}$$

$$\mathbb{C}^{-1} = \operatorname{sech}\frac{z\Psi_D}{2} + \Lambda_S, \tag{15b}$$

which are the classical GC relations.[11,12] For $a_+ \to 0$ and $a_+/a_- = 1$ but different ion valences, Equations (12) and (14) become

$$Q = \operatorname{sgn}(\Psi_D)\sqrt{\frac{2}{z_+ z_-}\left(\frac{z_+\exp\left(z_-\Psi_D\right) + z_-\exp\left(-z_+\Psi_D\right)}{z_+ + z_-} - 1\right)}, \tag{16a}$$

$$\mathbb{C}^{-1} = \frac{z_+ + z_-}{|\exp(z_-\Psi_D) - \exp(-z_+\Psi_D)|}\sqrt{\frac{2}{z_+ z_-}\left(\frac{z_+\exp(z_-\Psi_D) + z_-\exp(-z_+\Psi_D)}{z_+ + z_-} - 1\right)} + \Lambda_S, \tag{16b}$$

which are consistent with the results reported in reference 38. However, the results analogous to Equation (16) reported in 38 are presented in an awkward dimensional form. Taking the limit of $z_+ = z_- = z$ in Equation (16), it is easy to recover the GC relations in Equation (15). Lastly, for $z_+ = z_- = z$ and $a_+ = a_- = a$, Equations (12) and (14) are evaluated as

$$Q = \operatorname{sgn}(\Psi_D)\sqrt{\frac{1}{z^3a^3c_0}\ln\left(1 + 4za^3c_0\sinh^2\frac{z\Psi_D}{2}\right)}, \tag{17a}$$

$$\mathbb{C}^{-1} = \frac{1 + 4za^3c_0\sinh^2\dfrac{z\Psi_D}{2}}{|\sinh z\Psi_D|}\sqrt{\frac{1}{za^3c_0}\ln\left(1 + 4za^3c_0\sinh^2\frac{z\Psi_D}{2}\right)} + \Lambda_S, \tag{17b}$$

which agree with the relations presented in references 21, 28. We summarize the validity of aforementioned diffuse charge relations for $Q(\Psi_D)$ and $C(\Psi_D)$ in Table 1. To the best of our knowledge, Equations (12) and (14) are the most general charge and capacitance relations reported in literature accounting for ion valence and finite ion size.

Table 1: Summary of $Q(\Psi_D)$ and $\mathbb{C}(\Psi_D)$ relations that account for ion valence and finite ion size. For simplicity, we assume $\Lambda_S = 0$.

Conditions	Diffuse charge relations	References
$z_+ = z_- = z$ $a_\pm \to 0$	$Q = \frac{2}{z}\sinh\frac{z\Psi_D}{2}$ $\mathbb{C} = \cosh\frac{z\Psi_D}{2}$	11, 12
$z_+ \neq z_-$ $a_\pm \to 0$	$Q = \mathrm{sgn}(\Psi_D)\sqrt{\frac{2}{z_+ z_-}\left(\frac{z_+\exp\left(z_-\Psi_D\right)+z_-\exp\left(-z_+\Psi_D\right)}{z_+ + z_-} - 1\right)}$ $\mathbb{C} = \frac{\lvert\exp(z_-\Psi_D) - \exp(-z_+\Psi_D)\rvert}{(z_+ + z_-)\lvert Q\rvert}$	38, 40
$z_+ = z_- = z$ $a_+ = a_- = a$	$Q = \mathrm{sgn}(\Psi_D)\sqrt{\frac{1}{z^3a^3c_0}\ln\left(1 + 4za^3c_0\sinh^2\frac{z\Psi_D}{2}\right)}$ $\mathbb{C} = \frac{\lvert\sinh z\Psi_D\rvert}{z\left(1 + 4za^3c_0\sinh^2\frac{z\Psi_D}{2}\right)\lvert Q\rvert}$	20, 21, 28
$z_+ = z_- = z$ $a_+ \neq a_-$	$n_+ = \frac{\exp(-z\Psi)}{g(\Psi)}, n_- = \frac{\exp(z\Psi)f(\Psi)}{g(\Psi)}$ $f(\Psi) = \left(1 + \frac{za_-^3c_0\left(\exp\left(z\Psi\right)-1\right)}{1 - za_+^3c_0}\right)^{\frac{a_+^3}{a_-^3}-1}$ $g(\Psi) = f(\Psi) + za_+^3c_0\left(\exp(-z\Psi) - f(\Psi)\right) +$ $za_-^3c_0f(\Psi)\left(\exp(z\Psi)-1\right)$ $Q = \mathrm{sgn}(\Psi_D)\sqrt{\frac{1}{z^3a_+^3c_0}\ln g(\Psi_D)}$ $\mathbb{C} = \frac{\lvert n_-(\Psi_D) - n_+(\Psi_D)\rvert}{2z\lvert Q\rvert}$	29
$z_+ \neq z_-$ $a_+ \neq a_-$	$n_+ = \frac{\exp(-z_+\Psi)}{g(\Psi)}, n_- = \frac{\exp(z_-\Psi)f(\Psi)}{g(\Psi)}$ $f(\Psi) = \left(1 + \frac{z_+a_-^3c_0\left(\exp\left(z_-\Psi\right)-1\right)}{1 - z_-a_+^3c_0}\right)^{\frac{a_+^3}{a_-^3}-1}$ $g(\Psi) = f(\Psi) + z_-a_+^3c_0\left(\exp(-z_+\Psi) - f(\Psi)\right) +$ $z_+a_-^3c_0f(\Psi)\left(\exp(z_-\Psi)-1\right)$ $Q = \mathrm{sgn}(\Psi_D)\sqrt{\frac{2}{z_+z_-(z_+ + z_-)a_+^3c_0}\ln g(\Psi_D)}$ $\mathbb{C} = \frac{\lvert n_-(\Psi_D) - n_+(\Psi_D)\rvert}{(z_+ + z_-)\lvert Q\rvert}$	this work

Salt uptake

Both Q and $\mathbb{C}$ are measures of the net charge inside the double layer. However, the formation of a double layer also depletes salt from the bulk. As noted in references 3, 46, the amount of salt uptake directly dictates the dynamics of the double layer formation process, as explained later. We define the length scale of the bulk as L and estimate a dimensionless measure of the excess salt uptake as

$$\alpha = \frac{\int_0^\infty \left(c_+ + c_- - (z_+ + z_-)c_0\right) dx}{(z_+ + z_-)c_0 L}. \tag{18}$$

When $\alpha \ll 1$, the solution to double layer charging for an electrolyte between two parallel plates can be reliably approximated as an electrical circuit.[3] However, if $\alpha = \mathcal{O}(1)$, this approximation is no longer reliable. Therefore, estimation of α is important for time-dependent problems. To estimate α, we utilize Equations (7) and (11) to obtain

$$\alpha = \frac{\lambda_D}{L}\sqrt{\frac{a_+^3 c_0 z_+}{2(z_+ + z_-)}}\left|\int_0^{\Psi_D} \frac{z_-(n_+ - 1) + z_+(n_- - 1)}{\sqrt{\ln g(\Psi)}} d\Psi\right|, \tag{19}$$

where n_+, n_- and $g(\Psi)$ are evaluated from Equation (7). In the limit $a_+ \to 0$, $a_+/a_- = 1$, and $z_+ = z_- = z$, we recover the well-documented result[3] of $\alpha = \dfrac{4\lambda_D}{L}\sinh^2\dfrac{z\Psi_D}{4}$. We numerically integrate Equation (19) to evaluate the dependence of α on different parameters and the results are discussed later.

Potential Distribution $\Psi(X)$

We now discuss the numerical solution to Equation (11) with the Stern layer boundary condition (10a). We first report the effect of changes in $a_+^3 c_0$ on $\Psi(X)$ with $\Psi_0 = 5$, $z_+ = 1, z_- = 3$, $a_+/a_- = 1$ and $\Lambda_S = 0$; see Fig. 2(a). Physically, for a larger value of $a_+^3 c_0$, *i.e.* larger steric effects, $|Q|$ is smaller. Since $Q = -\left.\dfrac{d\Psi}{dX}\right|_{X=0}$, a larger $a_+^3 c_0$ implies a more gradual decrease in Ψ with X.

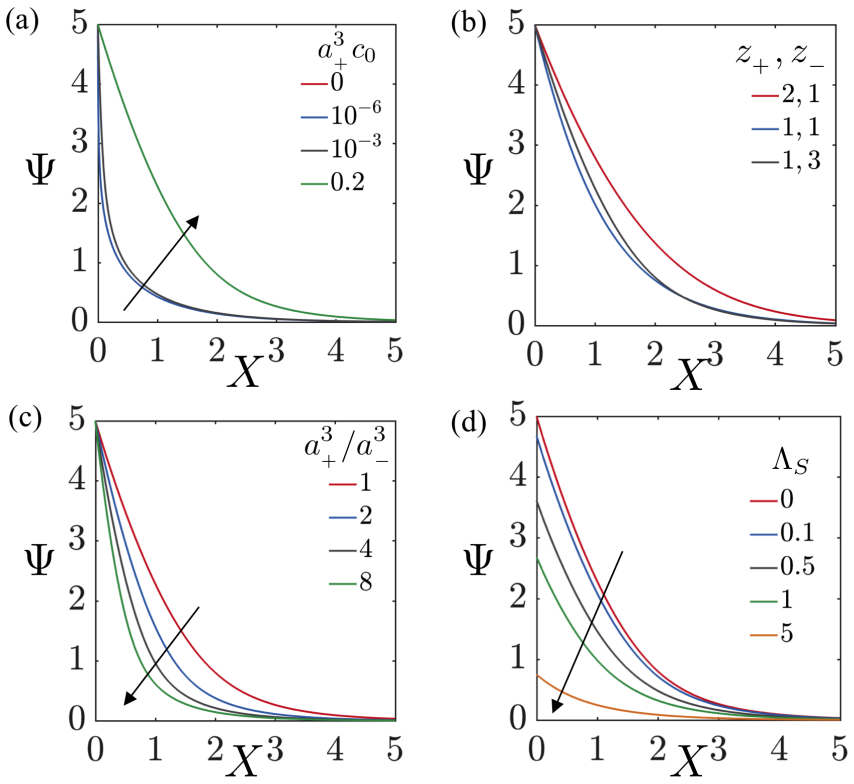

Figure 2: Effect of asymmetry in electrolyte valence on finite ion-size effects for $\Psi(X)$, as given by the numerical solution of Equation (11) with boundary condition (10a) for $\Psi_0 = 5$. (a) Different $a_+^3 c_0$ with $z_+ = 1$, $z_- = 3$, $a_+/a_- = 1$ and $\Lambda_S = 0$. (b) Different z_+ and z_- with $a_+^3 c_0 = 0.2$, $a_+/a_- = 1$ and $\Lambda_S = 0$. (c) Different a_+^3/a_-^3 with $z_+ = 1$, $z_- = 3$, $a_+^3 c_0 = 0.2$, and $\Lambda_S = 0$. (d) Different Λ_S with $z_+ = 1$, $z_- = 3$, $a_+^3 c_0 = 0.2$, and $a_+^3/a_-^3 = 1$.

The effect of change in z_+ and z_- on $\Psi(X)$ with $\Psi_0 = 5$, $a_+^3 c_0 = 0.2$, $a_+/a_- = 1$ and $\Lambda_S = 0$ is provided in Fig. 2(b). The trend shows that the fastest decay in Ψ occurs for $z_+ = z_- = 1$ whereas the decay is slowest for $z_+ = 2, z_- = 1$. Physically, for $a_+^3 c_0 = 0.2$, the ion concentration is high even in the bulk and thus finite ion-size effects are important. We assume that for $\Psi \approx 5$, $c_- \approx 1/a_-^3$, $z_+ c_+(0) \ll z_- c_-(0)$, and it can be estimated that $\dfrac{d\Psi}{dX} \approx -\sqrt{\dfrac{2\Psi}{z_+(z_+ + z_-)a_-^3 c_0}}$; see Equation (9). This approximation explains the trend we observe in Fig. 2(b). Similarly, for $z_+ = 1, z_- = 3$, $a_+^3 c_0 = 0.2$ and $\Lambda_S = 0$, we find that a smaller a_- increases the magnitude of $\left|\dfrac{d\Psi}{dX}\right|$, and thus the change in Ψ is more rapid for a smaller a_-, as observed in Fig. 2(c).

The effect of Λ_S on $\Psi(X)$ enters through the boundary condition (10a). We present the results of changes in Λ_S on $\Psi(X)$ with $\Psi_0 = 5$, $a_+^3 c_0 = 0.2$, $z_+ = 1$, $z_- = 3$ and $a_+/a_- = 1$ in Fig. 2(d). A thicker Stern layer, or a larger Λ_S, implies a larger potential drop across the Stern layer. Therefore, we see that $\Psi_D = \Psi(0)$ decreases for an increase in Λ_S. Further, a smaller Ψ_D indicates a lower $|Q|$ (see below), and thus for a larger Λ_S, the rate of decay of Ψ is smaller.

Charge accumulated

We present the dependence of accumulated charge Q on different parameters according to Equation (12). Fig. 3(a) shows the dependence of Q with Ψ_D for different values of $a_+^3 c_0$ with $z_+ = 1, z_- = 3$ and $a_+/a_- = 1$. A larger $a_+^3 c_0$ implies that steric effects are stronger, and thus Q is smaller. Increasing Ψ_D increases the concentration of ions and thus Q increases. For a large Ψ_D, steric effects start to become more important and the increase in Q is smaller since the rate of change in ion concentration is lower.

Next, we consider valence asymmetry for $a_+^3 c_0 = 0.2$ and $a_+/a_- = 1$. Since finite ion-size effects are significant here, for $\Psi_D > 0$, we assume $c_-(0) \approx 1/a_-^3$ and $z_+ c_+(0) \ll z_- c_-(0)$ to obtain

$$Q = -\left.\frac{d\Psi}{dX}\right|_{x=0} \approx \sqrt{\frac{2\Psi_D}{z_+(z_+ + z_-)a_-^3 c_0}}. \tag{20}$$

We find good agreement between computed values from Equation (12) and approximate values from Equation (20), especially for large $|\Psi_D|$ since concentration approximations are more accurate for large $|\Psi_D|$. Q is highest for $z_+ = z_- = 1$ followed by $z_+ = 1, z_- = 3$ and $z_+ = 2, z_- = 1$ (see Fig. 3(b)). Similarly, for $a_+^3 c_0 = 0.2$, $z_+ = 1$ and $z_- = 3$, a smaller a_- leads to a larger Q, as predicted by Equation (20). This observation is corroborated in Fig. 3(c). Lastly, Λ_S does not influence the variation of Q versus Ψ_D. However, for the same

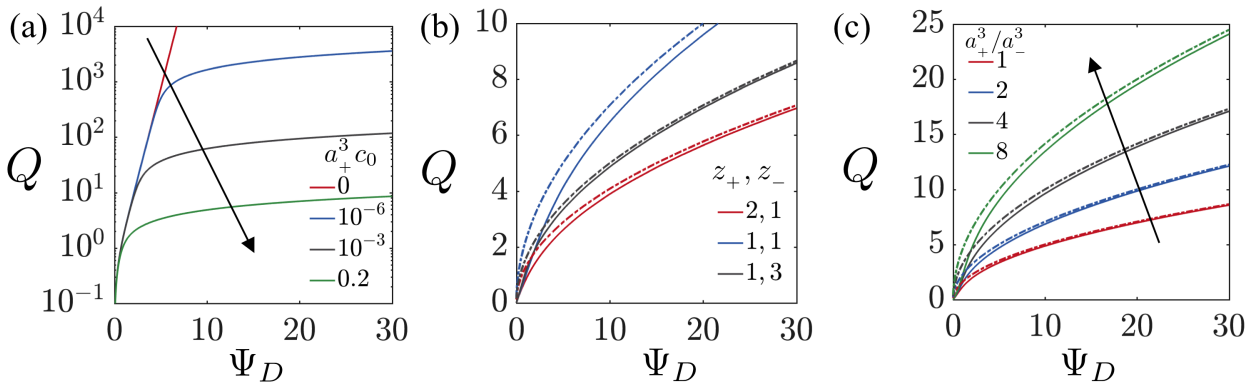

Figure 3: Effect of asymmetry in electrolyte valence on finite ion-size effects for $Q(\Psi_D)$, as given by the Equations (12) and (20). The solid lines represent results from Equation (12) and the dotted lines denote results from (20). (a) Different $a_+^3 c_0$ with $z_+ = 1$, $z_- = 3$ and $a_+/a_- = 1$. (b) Different z_+ and z_- with $a_+^3 c_0 = 0.2$ and $a_+/a_- = 1$. (c) Different a_+^3/a_-^3 with $z_+ = 1$, $z_- = 3$ and $a_+^3 c_0 = 0.2$.

value of Ψ_0, values of Ψ_D will be smaller for a larger Λ_S (Equation (10a), see Fig. 2(d)).

Capacitance

Capacitance $\mathbb{C}$ is a measure of the amount of charge stored per unit total potential drop, *i.e.* $\left|\frac{dQ}{d\Psi_0}\right|$. We discuss the dependence of $\mathbb{C}$ on different parameters based on Equation (14). Fig. 4(a) plots the variation of $\mathbb{C}$ with Ψ_D for different values of $a_+^3 c_0$ with $z_+ = 1, z_- = 3$, $a_+/a_- = 1$ and $\Lambda_S = 0$ as constants. Depending on the value of $a_+^3 c_0$, capacitance exhibits different behaviour.

For dilute ion concentrations in the bulk, *i.e.* $a_+^3 c_0 \lesssim \mathcal{O}(10^{-2})$, $\mathbb{C}$ (Ψ_D) displays a camel shape with one local minimum and two local maxima. Physically, this occurs because for small values of $|\Psi_D|$, counter ion concentration increases with increase in $|\Psi_D|$. For large values of $|\Psi_D|$, the counter ion concentration saturates around $\Psi_D = \Psi_{D,\max}$, beyond which the capacitance decreases. Fig. 4(a) shows that the curves are asymmetric when the cation and anion valences are not equal, or $\mathbb{C}(-\Psi_D) \neq \mathbb{C}(\Psi_D)$ for $z_+ \neq z_-$. We note that the location of the minimum $\Psi_D = \Psi_{D,\min} \neq 0$ for $z_+ = 1$ and $z_- = 3$, unlike valence symmetric

electrolytes. Similarly, the location of two maxima are not equal and opposite for unequal cation and anion valences.

For large bulk ion concentrations, *i.e.* $a_+^3 c_0 \gtrsim \mathcal{O}(10^{-1})$, $\mathbb{C}$ (Ψ_D) curves show a bell shape with no local minimum and one local maximum. Since the ion concentration is high even in bulk, the local minimum disappears and only one local maximum remains. We find that since cation and anion valences are unequal, $\Psi_{D,\max} \neq 0$. Though the camel shape and bell shape curves have been reported previously,[20] here we emphasize that the shapes and the $\Psi_{D,\max}$ and $\Psi_{D,\min}$ are significantly influenced by z_+ and z_-. In the subsequent subsection, we use a scaling analysis to detail a more quantitative estimate of extrema and their dependence on z_+ and z_-.

Next, we present the results for $a_+^3 c_0 = 0.2$, $a_+/a_- = 1$ and $\Lambda_S = 0$ but with different cation and anion valences in Fig. 4(b). We find that the position of a local maximum in the bell shape capacitance is also dictated by the valence and $\Psi_{D,\min} > 0$ when $z_- > z_+$ and $\Psi_{D,\min} < 0$ when $z_+ > z_-$. We note that an approximation for $\mathbb{C}$ is possible by assuming $c_+(0) \approx 1/a_+^3, z_- c_-(0) \ll z_+ c_+(0)$ for $\Psi_D < 0$ and $c_-(0) \approx 1/a_-^3, z_+ c_+(0) \ll z_- c_-(0)$ for $\Psi_D > 0$. We can estimate $\mathbb{C}$ by differentiating Equation (20) to obtain

$$\mathbb{C} \approx \left(2|\Psi_D| z_-(z_- + z_+) a_+^3 c_0\right)^{-1/2} \text{ for } \Psi_D < 0, \tag{21a}$$

$$\mathbb{C} \approx \left(2|\Psi_D| z_+(z_- + z_+) a_-^3 c_0\right)^{-1/2} \text{ for } \Psi_D > 0. \tag{21b}$$

Equation (21) is more accurate for large $a_\pm^3 c_0$ and $|\Psi_D|$ since the assumptions for ion concentrations are more readily satisfied. Therefore, Equation (21) predicts a decrease in $\mathbb{C}$ with an increase in $|\Psi_D|$ and does not predict the extrema near $\Psi_D = 0$. However, it correctly captures the trends and relative position of $\mathbb{C}$ reported in Fig. 4(b) for $|\Psi_D| \gtrsim \mathcal{O}(1)$ for different combinations of z_+ and z_-.

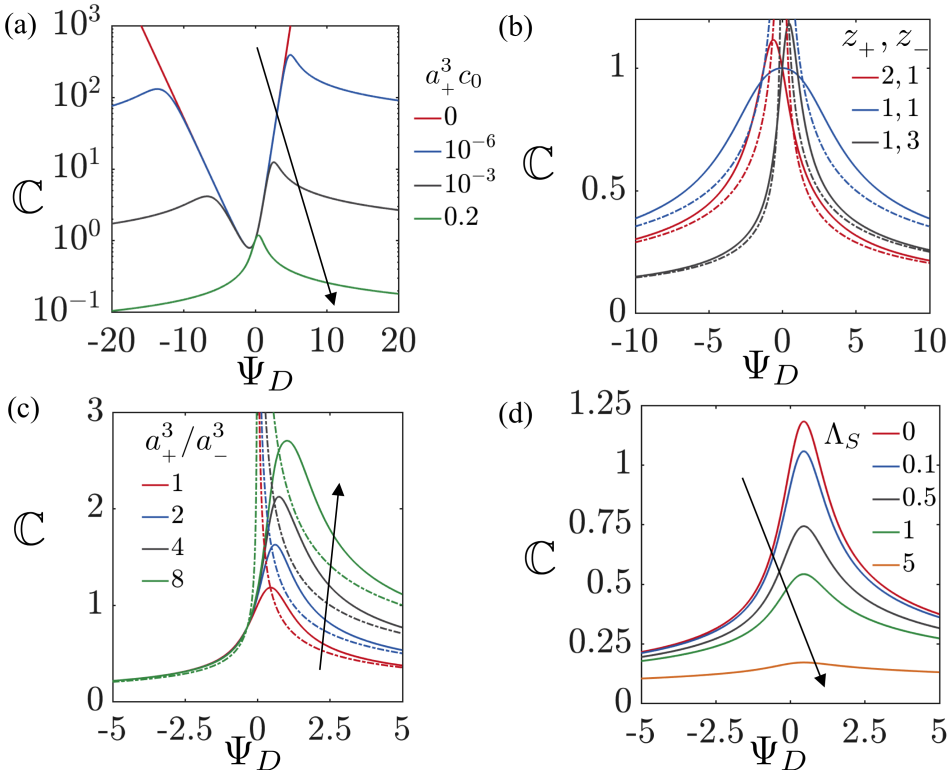

Figure 4: Effect of asymmetry in electrolyte valence on finite ion-size effects for $\mathbb{C}(\Psi_D)$, as given by the Equations (14) and (21). The solid lines represent results from Equation (14) and the dotted lines denote results from (21). (a) Different $a_+^3 c_0$ with $z_+ = 1$, $z_- = 3$, $a_+/a_- = 1$ and $\Lambda_S = 0$. (b) Different z_+ and z_- with $a_+^3 c_0 = 0.2$, $a_+/a_- = 1$ and $\Lambda_S = 0$. (c) Different a_+^3/a_-^3 with $z_+ = 1$, $z_- = 3$, $a_+^3 c_0 = 0.2$, and $\Lambda_S = 0$. (d) Different Λ_S with $z_+ = 1$, $z_- = 3$, $a_+^3 c_0 = 0.2$, and $a_+^3/a_-^3 = 1$.

We note that Equation (21) suggests that $\mathbb{C}$ also depends on a_+^3/a_-^3. Typical results are presented in Fig. 4(c) with $a_+^3 c_0 = 0.2$, $z_+ = 1$, $z_- = 3$ and $\Lambda_S = 0$ for different a_+^3/a_-^3. Equation (21) explains the collapse of curves for $\Psi_D < 0$ and the increase in $\mathbb{C}$ for higher a_+^3/a_-^3 for $\Psi_D > 0$.

Lastly, we discuss the effect of Λ_S. For different values of Λ_S, Fig. 4(d) presents the variation of $\mathbb{C}$ with Ψ_D for different with $a_+^3 c_0 = 0.2, z_+ = 1, z_- = 3$ and $a_+/a_- = 1$. We find that $\mathbb{C}$ decreases with an increase in Λ_S, and becomes almost independent of Ψ_D for larger values of Λ_S. This change in behavior occurs since the Stern layer capacitor and the diffuse layer

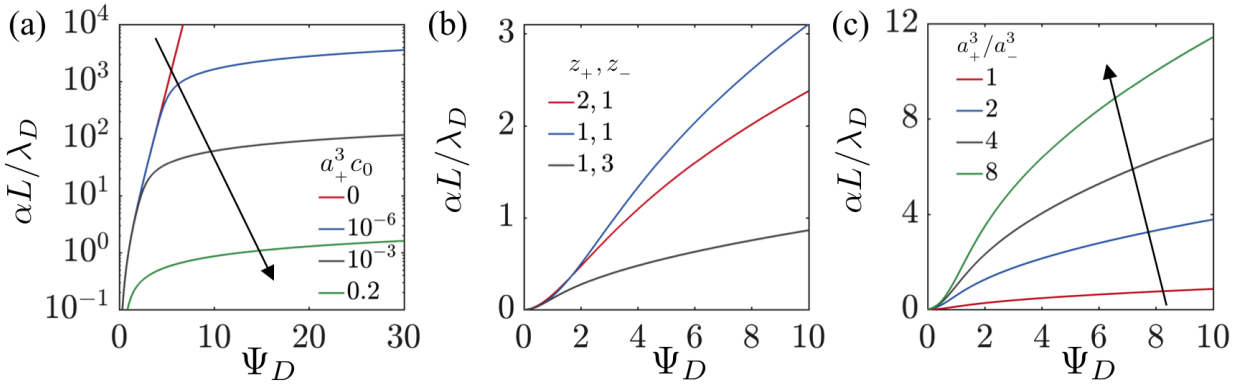

Figure 5: Effect of asymmetry in electrolyte valence on finite ion-size effects for $\alpha(\Psi_D)$, as given by the Equation (19). (a) Different $a_+^3 c_0$ with $z_+ = 1$, $z_- = 3$ and $a_+/a_- = 1$. (b) Different z_+ and z_- with $a_+^3 c_0 = 0.2$ and $a_+/a_- = 1$. (c) Different a_+^3/a_-^3 with $z_+ = 1$, $z_- = 3$ and $a_+^3 c_0 = 0.2$.

capacitor are in series; an increase in Λ_S results in the effective capacitance to be dictated by the Stern layer capacitance.

Salt uptake

In this section, we describe the variation of the dimensionless salt uptake $\alpha(\Psi_D)$ as given by Equation (19). As noted previously, α dictates the dynamics of double layer charging. Fig. 5(a) shows the dependence of α for different $a_+^3 c_0$ with $z_+ = 1$, $z_- = 3$ and $a_+^3/a_-{}^3 = 1$. As expected, an increase in $a_+^3 c_0$ decreases salt uptake since the ion concentration saturates due to finite ion-size effects.

In Fig. 5(b), we present the dependence of valence on salt uptake for $a_+^3 c_0 = 3$ and $a_+/a_- = 1$. We find that $\alpha\lambda_D/L$ is largest for $z_+ = 1, z_- = 1$ followed by $z_+ = 2, z_- = 1$ and $z_+ = 1, z_- = 3$. This trend occurs since for $\Psi_D > 0$, anion concentration saturates inside the double layer. This saturation occurs for smaller values of Ψ_D for $z_+ = 1, z_- = 3$ and thus lower salt is depleted from the bulk when compared to $z_+ = 2, z_- = 1$ and $z_+ = z_- = 1$. Further, though these two cases might achieve anion concentration saturation at similar values of Ψ_D, a larger number of anions in the bulk for $z_+ = 2, z_- = 1$ leads to a lower level of

salt depletion. Fig. 5(c) summarizes the effect of a_+^3/a_-^3 for $a_+^3 c_0 = 0.2$, $z_+ = 1$ and $z_- = 3$. We find that salt depletion is maximum for smaller values of a_- since the saturation concentration of anions is larger, and thus more salt can be depleted. A quantitative prediction of $\alpha(\Psi_D)$, similar to Equations (20) and (21) for Q and $\mathbb{C}$, is challenging since we need to find an approximate description for $d\psi/dx$ for all x (and not just at $x = 0$ as in Equations (20) and (21)); see Equation (18).

Scaling analysis

A unique feature of the derived diffuse-charge relations is the presence of extrema in the dependence of $\mathbb{C}$ with Ψ_D and their dependence on the values of z_+ and z_-. We now present physical arguments to predict the location of local extrema. Local maxima occur when the ion concentration inside the diffuse layer is on the order of $1/a_\pm^3$. For $\Psi_D > 0$, negative ions will be attracted and the condition for a local maximum implies $c_- = \mathcal{O}(1/a_-^3)$. On the other hand, for $\Psi_D < 0$, the condition for a local maximum becomes $c_+ = \mathcal{O}(1/a_+^3)$. Thus, assuming the $c_\pm$ follow the Boltzmann distribution, we estimate

$$z_- c_0 \exp(-z_+ \Psi_{D,\max}) = \mathcal{O}(1/a_+^3) \text{ for } \Psi_D \leq 0, \tag{22a}$$

$$z_+ c_0 \exp(z_- \Psi_{D,\max}) = \mathcal{O}(1/a_-^3) \text{ for } \Psi_D \geq 0, \tag{22b}$$

or

$$\Psi_{D,\max} = \mathcal{O}\left(z_+^{-1} \ln(z_- a_+^3 c_0)\right) \text{ for } \Psi_D \leq 0, \tag{23a}$$

$$\Psi_{D,\max} = -\mathcal{O}\left(z_-^{-1} \ln(z_+ a_-^3 c_0)\right) \text{ for } \Psi_D \geq 0. \tag{23b}$$

Equation (23) demonstrates that $\Psi_{D,\max}$ is strongly influenced by z_+ and z_-. We observe a good quantitative agreement between the predictions of Equation (23) and the computed values (obtained from Equation (14)), as illustrated in Fig. 6(a,b). The scaling relations

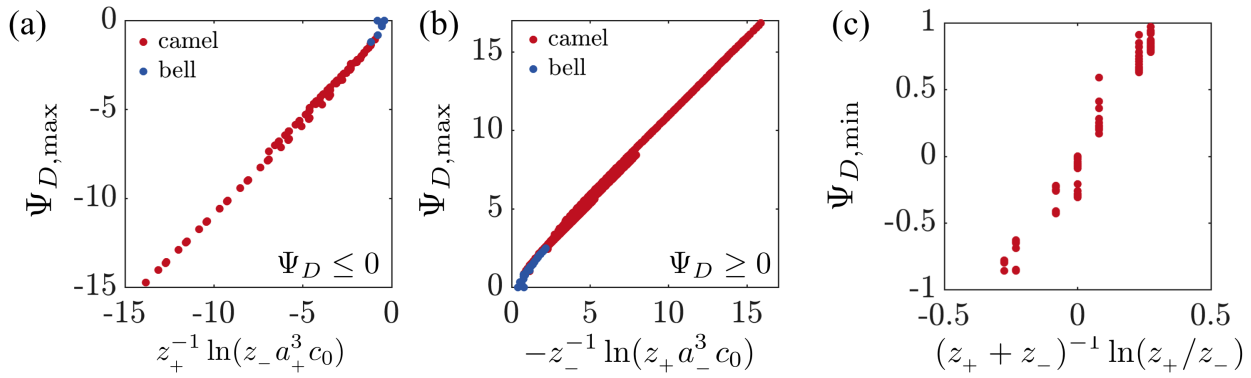

Figure 6: Scaling analysis of finite ion-size effects. Comparison of computed $\Psi_{D,\max}$ with Equation (23) for (a) $\Psi_D < 0$ and (b) $\Psi_D > 0$. (c) Comparison of computed $\Psi_{D,\min}$ with Equation (24). The red points are cases with the camel shape, *i.e.* two local maxima and one local minima, and the blue points are cases with the bell shape, *i.e.* one local maximum. For computations, $10^{-6} \leq a_+^3 c_0 \leq 0.2$, $1 \leq a_+^3/a_-^3 \leq 8$, $1 \leq z_+ \leq 3$, and $1 \leq z_- \leq 3$.

accurately capture the behavior, especially for the camel-shape capacitance curves, *i.e.* with two local maxima and one local minima. However, the scaling relation is not as accurate for the bell shape capacitance curves, *i.e.* only one local maximum and no local minimum, since the assumption that concentration follows a Boltzmann distribution is less accurate. Nevertheless, Equation (23) correctly captures the dependence of $\Psi_{D,\max}$ on z_+, z_-, $a_+^3 c_0$, and a_+/a_-.

We now present a physical argument to predict $\Psi_{D,\min}$ which is only observed in the camel-shape capacitance curves. We know that the magnitude of charge per unit volume carried by the cations and anions is proportional to $z_+ c_+$ and $z_- c_-$ respectively. For instance, in bulk, by definition, $z_+ c_+ = z_- c_-$, and the charges balance. However, the magnitude of the rate of change in charge with Ψ_D of cations and anions is proportional to $z_+^2 c_+$ and $z_-^2 c_-$ (assuming the Boltzmann distribution, see Equation (7)). We argue that $\Psi_{D,\min}$ can be estimated when $\dfrac{z_+^2 c_+}{z_-^2 c_-} = \mathcal{O}(1)$. Assuming the Boltzmann distribution, this condition yields

$$\Psi_{D,\min} = \mathcal{O}\left(\frac{\ln(z_+/z_-)}{z_+ + z_-}\right). \tag{24}$$

Therefore, physically, $\Psi_{D,\min}$ is the potential at which the rate of change of both positive and negative charges with Ψ_D are equal. Due to symmetry, this occurs at $\Psi_D = 0$ for $z_+ = z_- = 1$. We show that predictions of Equation (24) are in good agreement with computed results (obtained from Equation (14)) in Fig. 6(c).

Physical significance

We now discuss the physical significance and implications of valence asymmetry of finite ion-size effects. For this discussion, we briefly restore dimensions for charge $q(\psi_D)$ and capacitance $\mathfrak{c}(\psi_D)$. By converting Equations (20) and (21) to dimensional form, we obtain

$$q \approx -\left(2\varepsilon_0\varepsilon_s z_+ a_+^{-3}|\psi_D|\right)^{1/2} \text{ for } \psi_D < 0, \tag{25a}$$

$$q \approx \left(2\varepsilon_0\varepsilon_s z_- a_-^{-3}|\psi_D|\right)^{1/2} \text{ for } \psi_D > 0, \tag{25b}$$

$$\mathfrak{c} \approx \left(0.5\varepsilon_0\varepsilon_s z_+ a_+^{-3}|\psi_D|^{-1}\right)^{1/2} \text{ for } \psi_D < 0, \tag{25c}$$

$$\mathfrak{c} \approx \left(0.5\varepsilon_0\varepsilon_s z_- a_-^{-3}|\psi_D|^{-1}\right)^{1/2} \text{ for } \psi_D > 0. \tag{25d}$$

Equation (25) clearly shows that $q(\psi_D) = q(-\psi_D)$ and $\mathfrak{c}(\psi_D) = \mathfrak{c}(-\psi_D)$ only when $z_+ a_+^{-3} = z_- a_-^{-3}$. Physically speaking, z_+/a_+^3 and z_-/a_-^3 are, respectively, a measure of the maximum positive charge density and negative charge density that can be stored inside the double layers. Therefore, the condition $z_+ a_+^{-3} = z_- a_-^{-3}$ implies that the double layer formation is symmetric only when the magnitude of maximum charge densities accumulated inside the double layer are the same irrespective of the sign of the potential drop. Moreover, the individual factors $z_+ a_+^{-3}$ and $z_- a_-^{-3}$ combine the relative importance of ion valence and finite ion size, and suggest that a higher valence and a lower ionic diameter increases the amount of charge stored and the capacitance. This result is consistent with physical intuition since increasing the valence increases the magnitude of force that attracts the ion towards the charged surface and a smaller ion size allows for a larger number of ions per unit volume to accumulate in the double layer. Moreover, the square root dependence highlights a quanti-

tative feature that is important for practical applications. As an example, we consider the case of $CaCl_2$, which is a possible electrolyte candidate for supercapacitors,[44] among many applications. For this salt, $z_+ = 2$, $z_- = 1$, $a_+ = 0.11$ nm and $a_- = 0.17$ nm. Here, the factor $\left(\frac{z_+ a_+^{-3}}{z_- a_-^{-3}}\right)^{1/2} = 2.71$, which informs us that for the same magnitude potential drop across the charged surface, when the surface is negatively charged, the double layer will accumulate almost thrice as much net charge. This breaking of symmetry is significant and is important for supercapacitor applications where the amount of charge stored dictates the energy density. We note that the asymmetry in the double layer properties that arise (or are reduced) due to asymmetry in ion valence is the novel aspect of this work and creates opportunities for future research.

Dielectric decrement effect

In this section, we relax the assumption of a constant dielectric constant, *i.e.* $\varepsilon = \varepsilon_0 \varepsilon_s$. As previously discussed, changes in the dielectric constant with ion concentration can reduce the ability to store charge inside a double layer, and thus this effect can have a major impact on diffuse layer properties. Here, we assume that the decrease in the dielectric constant is linear with ion concentrations, or

$$\varepsilon(c_\pm) = \varepsilon_s - \gamma_+ c_+ - \gamma_- c_-, \tag{26}$$

where $\gamma_\pm$ are constants. Though Equation (26) is not obtained from a theoretical derivation, experiments have shown that this dependence works reasonably well for ion concentration up to a few molars.[32,34,48] Typical values of $\gamma_\pm$ range from $\gamma_\pm = \mathcal{O}(10^{-27} - 10^{-26})$ m^{-3} (see authors 32).

Derivation

To derive charge and capacitance relationships for a variable dielectric constant, Equations (3 - 5) remain identical except ε_s is replaced by $\varepsilon(c_\pm)$, as given by Equation (26). Due to the dependence of the dielectric constant on $c_\pm$, the chemical potentials $\mu_\pm$ also have a dependence on ε, or

$$\mu_+ = \frac{\partial F}{\partial c_+} = -\frac{\varepsilon_0}{2}\frac{\partial \varepsilon}{\partial c_+}\left|\frac{d\psi}{dx}\right|^2 + z_+ e\psi + k_B T\left[\ln\left(\frac{a_+^3 c_+}{1-a_+^3 c_+}\right) - \frac{a_+^3}{a_-^3}\ln\left(\frac{1-a_+^3 c_+ - a_-^3 c_-}{1-a_+^3 c_+}\right)\right], \quad (27a)$$

$$\mu_- = \frac{\partial F}{\partial c_-} = -\frac{\varepsilon_0}{2}\frac{\partial \varepsilon}{\partial c_-}\left|\frac{d\psi}{dx}\right|^2 - z_- e\psi + k_B T\ln\left(\frac{a_-^3 c_-}{1-a_+^3 c_+ - a_-^3 c_-}\right). \quad (27b)$$

Though it is possible to find an explicit relationship for concentration by equating $\mu_\pm(x) = \mu_\pm(\infty)$, the presence of $\left|\frac{d\psi}{dx}\right|^2$ in Equation (27) make the expression inconvenient. Therefore, we exploit the relationships built in references 32–34 for osmotic pressure $\pi(x)$, *i.e.*

$$\pi(x) = -\frac{\varepsilon_0 \varepsilon}{2}\left|\frac{d\psi}{dx}\right|^2 - z_+ e c_+ \psi + z_- e c_- \psi + TS + c_+\mu_+ + c_-\mu_-. \quad (28)$$

Using Equation (5), (26) and (27) in Equation (28) yields

$$\begin{aligned}\pi(x) = -\frac{\varepsilon_0}{2}\left(\varepsilon_s - 2\gamma_+ c_+ - 2\gamma_- c_-\right)\left|\frac{d\psi}{dx}\right|^2 \\ -k_B T\left(\frac{1}{a_-^3}\ln\left(1-a_+^3 c_+ - a_-^3 c_-\right) + \left(\frac{1}{a_+^3} - \frac{1}{a_-^3}\right)\ln\left(1-a_+^3 c_+\right)\right).\end{aligned} \quad (29)$$

Furthermore, utilizing the equilibrium requirements $\pi(x) = \pi(\infty)$ and $\mu_\pm(x) = \mu_\pm(\infty)$, we obtain three equations to relate $c_\pm(x)$, $\psi(x)$, and $\left|\frac{d\psi}{dx}\right|^2$. Thus, using these three equations at $x = 0$, we can evaluate $c_\pm(\psi_D)$ and $\left|\frac{d\psi}{dx}\right|(\psi_D)$, and by extension evaluate $q(\psi_D)$ and $\mathfrak{c}(\psi_D)$. To simplify our calculations, we assume that steric effects and Stern layer effects are negligible. However, as clear from the above derivation, no such restriction is necessary and the results can also be evaluated for the general scenario. We note that since we have used

osmotic pressure to generate an additional relationship, we have not utilized Gauss's law with variable dielectric constant.

We first evaluate $\pi(x) = \pi(\infty)$ and $\mu_\pm(x) = \mu_\pm(\infty)$ in the absence of steric effects, *i.e.* in the limit $a_+^3 c_0 \to 0$ and $a_+/a_- = 1$. Consistent with the earlier discussion, we define dimensionless variables as $n_+ = \dfrac{c_+}{z_- c_0}$, $n_- = \dfrac{c_-}{z_+ c_0}$, $X = \dfrac{x}{\lambda_D}$, and $\Psi = \dfrac{e\psi}{k_B T}$, and obtain

$$\left|\frac{d\Psi}{dX}\right|^2 = \frac{2\varepsilon_s(z_-(n_+ - 1) + z_+(n_- - 1))}{(z_+ + z_-)z_+ z_-(\varepsilon_s - 2\gamma_+ c_0 z_- n_+ - 2\gamma_- c_0 z_+ n_-)}, \tag{30a}$$

$$\gamma_+ c_0 \left(\frac{z_-(n_+ - 1) + z_+(n_- - 1)}{\varepsilon_s - 2\gamma_+ c_0 z_- n_+ - 2\gamma_- c_0 z_+ n_-}\right) + z_+\Psi + \ln(n_+) = 0, \tag{30b}$$

$$\gamma_- c_0 \left(\frac{z_-(n_+ - 1) + z_+(n_- - 1)}{\varepsilon_s - 2\gamma_+ c_0 z_- n_+ - 2\gamma_- c_0 z_+ n_-}\right) - z_-\Psi + \ln(n_-) = 0. \tag{30c}$$

Equation (30) is governed by the dimensionless parameters $z_\pm, \gamma_+ c_0, \gamma_+/\gamma_-$ and ε_s. We solve Equation (30) numerically for specified values of $\Psi(0) = \Psi_D$, $z_\pm$, $\gamma_+ c_0$, γ_+/γ_- and $\varepsilon_s = 80$ (typical of water), and obtain the functions $n_\pm(\Psi_D)$ and $\left|\dfrac{d\Psi}{dX}\right|(\Psi_D)$.

Once we have obtained $\left|\dfrac{d\Psi}{dX}\right|(\Psi_D)$, it is straightforward to obtain $\Psi(X)$ through numerical integration. Next, we evaluate $Q = -\dfrac{(\varepsilon_s - \gamma_+ c_0 z_- n_+ - \gamma_- c_0 z_+ n_-)}{\varepsilon_s}\left.\dfrac{d\Psi}{dX}\right|_{X=0}$. Moreover, since we assume $\Lambda_S = 0$, then $\Psi_0 = \Psi_D$ (see Equation (10a)), and $\mathbb{C} = \left|\dfrac{dQ}{d\Psi_D}\right|$, which is evaluated through numerical differentiation. We also numerically calculate the dimensionless salt uptake as $\alpha = \dfrac{\lambda_D}{L}\left|\displaystyle\int_0^{\Psi_D} \frac{z_-(n_+ - 1) + z_+(n_- - 1)}{(z_+ + z_-)\dfrac{d\Psi}{dX}} d\Psi\right|$. We note that though Equation (30) has been derived in the limit $a_\pm \to 0$ and $a_+ = a_-$, the results are readily extended to the general case. Also, we find that in the limit $\gamma_+ c_0 \to 0$ and $\gamma_+/\gamma_- = 1$ (the absence of the dielectric decrement), Equation (30) gives results consistent with Equation (16).

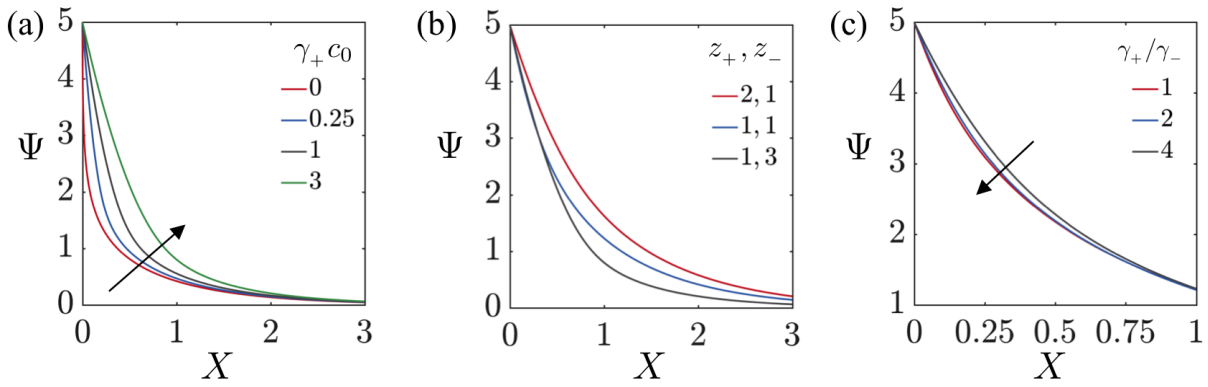

Figure 7: Effect of asymmetry in electrolyte valence on dielectric decrement for $\Psi(X)$, as given by the solution of Equation (30) for $\Psi_D = 5$. (a) Effect of $\gamma_+ c_0$ with $z_+ = 1$, $z_- = 3$ and $\gamma_+/\gamma_- = 1$. (b) Effect of z_+ and z_- with $\gamma_+ c_0 = 3$ and $\gamma_+/\gamma_- = 1$. (c) Effect of γ_+/γ_- with $\gamma_+ c_0 = 3$ with $z_+ = 1$ and $z_- = 3$. $\varepsilon_s = 80$ is assumed for all calculations.

Potential

We present the variation of $\Psi(X)$ for $\Psi_D = 5$ in Fig. 7. First, we discuss the effect of the change in $\gamma_+ c_0$ with $z_+ = 1$, $z_- = 3$ and $\gamma_+/\gamma_- = 1$. The change in $\Psi(X)$ is less rapid with an increase in $\gamma_+ c_0$ as shown in Fig. 7(a). In the dielectric decrement effect, much like the finite-ion size effect, the concentration of the counter ion saturates beyond some $|\Psi_D|$. Here, the saturation occurs because the lowering of the dielectric constant implies that the charge storage capacity of the solution is reduced, and thus the concentration of the counter ion saturates. Since it is difficult to parse the dependence of different parameters from Equation (30a), we present a simplified model to understand the effect of the dielectric decrement.

Since $\Psi_D > 0$, we assume that $z_+ c_+(0) \ll z_- c_-(0)$ and $\left|\dfrac{dc_-}{dx}\right|_{x=0} = 0$. These assumptions physically imply that majority of the repelled ions have been depleted and that the dielectric decrement leads to a saturation of the counter ions at the surface, and thus the gradient of the counter ion vanishes. These assumptions allow us to simplify Gauss's law at $x = 0$ as

$$\frac{d}{dx}\left(\varepsilon_0 \varepsilon(c_\pm)\frac{d\psi}{dx}\right)\bigg|_{x=0} = e(z_- c_- - z_+ c_+)\big|_{x=0} \implies \varepsilon_0 \varepsilon_s \frac{d^2\psi}{dx^2}\bigg|_{x=0} \approx z_- e c_-\big|_{x=0}\,. \tag{31}$$

Next, we invoke the chemical potential equality $\mu_-(x) = \mu_-(\infty)$ with $a_\pm \to 0$ in Equation (26) and (27b) to get

$$\frac{\varepsilon_0 \gamma_-}{2} \left| \frac{d\psi}{dx} \right|^2 - z_- e \psi_D + k_B T \ln \left(\frac{c_-(x)}{z_+ c_0} \right) \approx 0. \tag{32}$$

We differentiate Equation (32) with respect to x and utilize Equation (31) to evaluate $c_-(0)$ and $\left.\frac{d\psi}{dx}\right|_{x=0}$ as

$$c_-(0) \approx \frac{\varepsilon_s}{2\gamma_-}, \tag{33a}$$

$$\varepsilon(c_-(0)) \approx \varepsilon_s/2, \tag{33b}$$

$$\left.\frac{d\psi}{dx}\right|_{x=0} \approx -\mathrm{sgn}(\psi_D) \sqrt{\frac{2\left(z_- e \psi_D - k_B T \ln\left(\frac{\varepsilon_s}{2\gamma_- z_+ c_0} \right) \right)}{\varepsilon_0 \gamma_-}}. \tag{33c}$$

Non-dimensionalizing Equation (33c) we arrive at

$$\left.\frac{d\Psi}{dX}\right|_{X=0} \approx -\mathrm{sgn}(\Psi_D) \sqrt{\frac{2\varepsilon_s \left(\Psi_D - \frac{1}{z_-} \ln\left(\frac{\varepsilon_s}{2\gamma_- z_+ c_0} \right) \right)}{z_+(z_+ + z_-)\gamma_- c_0}}. \tag{34}$$

We emphasize that Equation (34) is an approximation and assumes that $z_+ c_+(0) \ll z_- c_-(0)$ and $\left.\left|\frac{dc_-}{dx}\right|\right|_{x=0} = 0$. Moreover, the argument inside the square root needs to be positive, or $\Psi_D > \frac{1}{z_-} \ln\left(\frac{\varepsilon_s}{2\gamma_- z_+ c_0} \right)$, and thus the relation is only applicable for large Ψ_D. However, there are useful insights to be gained from (34). The equation suggests that increasing $\gamma_- c_0$ leads to a more gradual decay in Ψ, consistent with the numerical observations in Fig. 7(a).

The variation of Ψ with z_+ and z_- is presented in Fig. 7(b) for $\gamma_+ c_0 = 3$ and $\gamma_+/\gamma_- = 1$. From Equation (34), we learn that $\left.\frac{d\Psi}{dX}\right|_{X=0}$ is largest for $z_+ = 1, z_- = 1$, followed by $z_+ = 1, z_- = 3$ and $z_+ = 2, z_- = 1$. This trend is consistent with the results shown in Fig. 7(b). However, Equation (34) is only valid at $X = 0$ and the variation in Ψ for other values of X are not

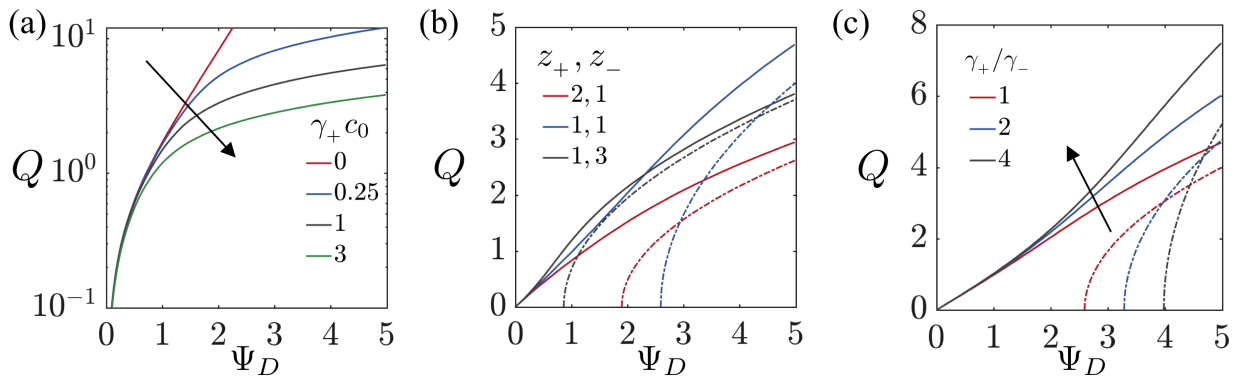

Figure 8: Effect of asymmetry in electrolyte valence on dielectric decrement for $Q(\Psi_D)$, as given by the solution of Equations (30) and (35). The solid lines represent results from Equation (30) and the dotted lines denote results from (35). (a) Effect of $\gamma_+ c_0$ with $z_+ = 1$, $z_- = 3$ and $\gamma_+/\gamma_- = 1$. (b) Effect of z_+ and z_- with $\gamma_+ c_0 = 3$ and $\gamma_+/\gamma_- = 1$. (c) Effect of γ_+/γ_- with $\gamma_+ c_0 = 3$ with $z_+ = 1$ and $z_- = 1$. $\varepsilon_s = 80$ is assumed for all calculations.

captured in Equation (34). Nonetheless, the results in Fig. 7(b) and Equation (34) clearly show that $\Psi(X)$ depends on the cation and anion valence. Next, we discuss the effect of γ_+/γ_- with $\gamma_+ c_0 = 3$, $z_+ = 1$ and $z_- = 3$. We observe in Fig. 7(c) that an increase in γ_+/γ_- leads to a more rapid decay in Ψ with X, although the difference is relatively minor. This observation is consistent with the prediction of Equation (34).

Charge accumulated

We now discuss the dependence of the charge accumulated Q on Ψ_D. Since the dielectric decrement saturates the counter ion concentration, an increase in $\gamma_+ c_0$ reduces Q; see Fig. 8(a) where the trends are presented for $z_+ = 1$, $z_- = 3$ and $\gamma_+/\gamma_- = 1$. By utilizing Equation (33), we predict

$$Q \approx \operatorname{sgn}(\Psi_D)\sqrt{\frac{\varepsilon_s\left(\Psi_D - \frac{1}{z_-}\ln\left(\frac{\varepsilon_s}{2\gamma_- z_+ c_0}\right)\right)}{2z_+(z_+ + z_-)\gamma_- c_0}}, \text{ for } \Psi_D > \frac{1}{z_-}\ln\left(\frac{\varepsilon_s}{2\gamma_- z_+ c_0}\right). \tag{35}$$

Equation (35) shows that increasing γ_- reduces Q, consistent with the trends observed in Fig. 8(a). The dependence of Q on z_+ and z_- is presented in Fig. 8(b). We find qualitative

agreement between the computed values from Equation (30) with the predictions of Equation (35). Fig. 8(c) shows the variation of Q on γ_+/γ_- for $\gamma_+ c_0 = 3$, $z_+ = 1$ and $z_- = 3$. The results suggest a larger Q for a smaller γ_-, qualitatively consistent with the prediction of Equation (35). The disagreement between the solutions from Equations (30) and (35) occur since the approximation of $z_+ c_+(0) \ll z_- c_-(0)$ and $c_-(0) \approx \dfrac{\varepsilon_s}{2\gamma_-}$ is more accurate for $\Psi_D = \mathcal{O}(10)$. Nonetheless, Equation (35) provides a convenient analytical expression to infer the dependence of different parameters on Q.

Capacitance

We now focus on the dependence of capacitance $\mathbb{C}$ on Ψ_D. Fig. 9(a) shows the dependence of $\mathbb{C}$ on $\gamma_+ c_0$ for $z_+ = 1, z_- = 3$ and $\gamma_+/\gamma_- = 1$. First, we note that for $\gamma_+ c_0 = 0$, *i.e.* no dielectric decrement, $\mathbb{C}$ has only one local minimum at $\Psi_D = \Psi_{D,\min} < 0$. This response has been described in detail in the previous section; see Equation (24). We observe that increase in $\gamma_+ c_0$ leads to a decrease in $\mathbb{C}$. In addition, with finite dielectric decrement, we start observing a maximum in $\mathbb{C}$ for $\Psi_D = \Psi_{D,\max}$, leading to the camel shape curves. For very large $\gamma_+ c_0$, we find that $\Psi_{D,\min}$ disappears and only one of the maxima $\Psi_{D,\max}$ remains, leading to a bell shape curve, similar to the finite-ion size effects (see Fig. 4(a)). However, increase in $\gamma_+ c_0$ also influences the $\mathbb{C}$ at $\Psi_D = 0$ unlike the increase in $a_+^3 c_0$ for finite-ion size effects; see Fig. 4(a).

To understand the capacitance response more quantitatively, we build on our simplified model for dielectric decrement. Here, we assume that for $\Psi_D > 0$, $z_+ c_+(0) \ll z_- c_-(0)$ and $c_-(0) \approx \dfrac{\varepsilon_s}{2\gamma_-}$ (see Equation (33)), and thus by extension for $\Psi_D < 0$, $z_- c_-(0) \ll z_+ c_+(0)$and $c_+(0) \approx \dfrac{\varepsilon_s}{2\gamma_+}$. Based on these assumptions, we previously derived $Q(\Psi_D)$ (see Equation (35))

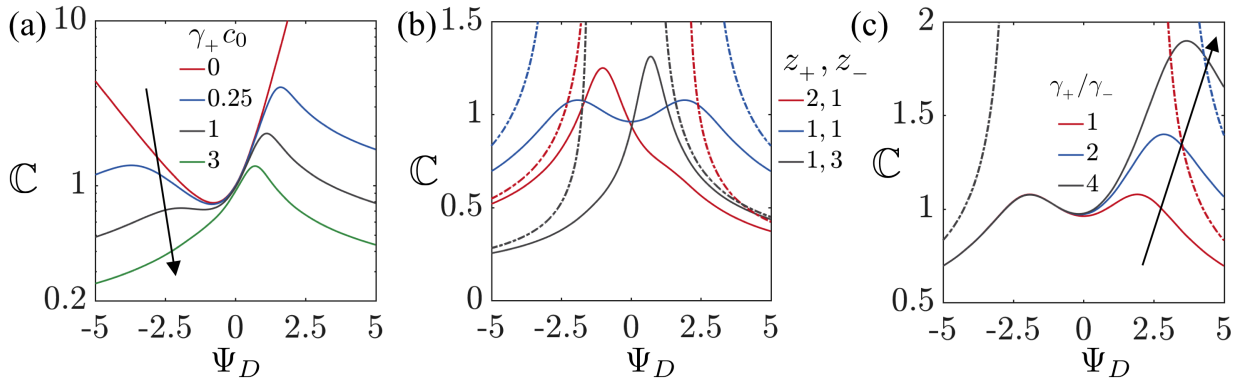

Figure 9: Effect of asymmetry in electrolyte valence on dielectric decrement for $\mathbb{C}(\Psi_D)$, as given by the solution of Equations (30) and (36). The solid lines represent results from Equation (30) and the dotted lines denote results from (36). (a) Effect of $\gamma_+ c_0$ with $z_+ = 1$, $z_- = 3$ and $\gamma_+/\gamma_- = 1$. (b) Effect of z_+ and z_- with $\gamma_+ c_0 = 3$ and $\gamma_+/\gamma_- = 1$. (c) Effect of γ_+/γ_- with $\gamma_+ c_0 = 3$ with $z_+ = 1$ and $z_- = 1$. $\varepsilon_s = 80$ is assumed for all calculations.

and $\mathbb{C} = \left|\dfrac{dQ}{d\Psi_D}\right|$ is thus calculated as

$$\varepsilon_s^2 \mathbb{C}^{-1} \approx 8 z_-(z_+ + z_-)\gamma_+ c_0 \left(|\Psi_D| - \frac{1}{z_+}\ln\left(\frac{\varepsilon_s}{2\gamma_+ z_- c_0}\right)\right) \text{ for } -\Psi_D > \frac{1}{z_+}\ln\left(\frac{\varepsilon_s}{2\gamma_+ z_- c_0}\right),$$
$$\varepsilon_s^2 \mathbb{C}^{-1} \approx 8 z_+(z_+ + z_-)\gamma_- c_0 \left(|\Psi_D| - \frac{1}{z_-}\ln\left(\frac{\varepsilon_s}{2\gamma_- z_+ c_0}\right)\right) \text{ for } \Psi_D > \frac{1}{z_-}\ln\left(\frac{\varepsilon_s}{2\gamma_- z_+ c_0}\right). \tag{36}$$

We investigate the effect of z_+ and z_- on $\mathbb{C}$ for $\gamma_+ c_0 = 3$ and $\gamma_+/\gamma_- = 1$ in Fig. 9(b). We find that changes in z_+ and z_- creates asymmetry in the capacitance curves. We are able to qualitatively capture the asymmetry and relative positions for different combinations of z_+ and z_- in Equation (36). However, Equation (36) does not predict a maximum and suggests that $\mathbb{C}$ is a strictly decreasing function with $|\Psi_D|$. This discrepancy between the computed results from Equation (30) and approximated results from Equation (36) arise due since the assumptions of cation and anion concentration are less accurate for $|\Psi_D| \lesssim \mathcal{O}(1)$. In Fig. 9(c), we describe the dependence of $\mathbb{C}$ with Ψ_D for different γ_+/γ_-, $\gamma_+ c_0 = 3$, $z_+ = 1$, and $z_- = 3$. We find that decreasing γ_- increases $\mathbb{C}$ for $\Psi_D > 0$ whereas keeping γ_+ constant collapses curves for $\Psi_D < 0$, consistent with the prediction of Equation (36).

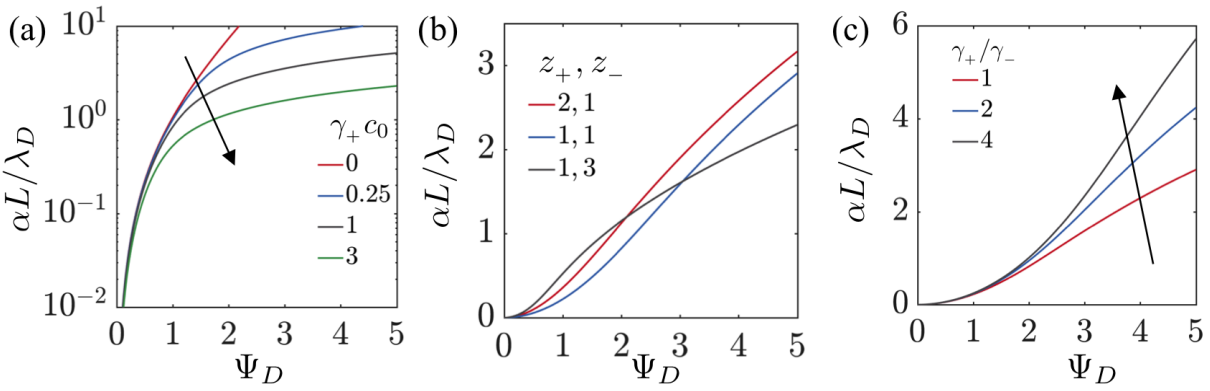

Figure 10: Effect of asymmetry in electrolyte valence on dielectric decrement for $\alpha(\Psi_D)$, as given by the solution of Equation (30). (a) Effect of $\gamma_+ c_0$ with $z_+ = 1$, $z_- = 3$ and $\gamma_+/\gamma_- = 1$. (b) Effect of z_+ and z_- with $\gamma_+ c_0 = 3$ and $\gamma_+/\gamma_- = 1$. (c) Effect of γ_+/γ_- with $\gamma_+ c_0 = 3$, $z_+ = 1$ and $z_- = 1$. $\varepsilon_s = 80$ is assumed for all calculations.

Salt uptake

An overview of the effect of dielectric decrement on dimensionless salt uptake is provided in Fig. 10. First, we focus on the effect of $\gamma_+ c_0$ for $z_+ = 1$, $z_- = 3$, and $\gamma_+/\gamma_- = 1$. We observe in Fig. 10(a) that an increase in $\gamma_+ c_0$ decreases $\alpha L/\lambda_D$. This response is expected since an increase in dielectric decrement leads to a larger saturation of ion concentration and thus less salt is absorbed in the diffuse layer. Fig. 10(b) presents the variation of $\alpha L/\lambda_D$ on z_+ and z_-. Based on our analysis for finite-ion size effects, here also, we expect $\alpha L/\lambda_D$ to be lowest for $z_+ = 1, z_- = 3$ since saturation would occur at the smallest value of Ψ_D. However, we find a different trend in Fig. 10(b). Though $\alpha L/\lambda_D$ for $z_+ = 1, z_- = 3$ does become lowest for large Ψ_D, it is maximum for small Ψ_D. Furthermore, $\alpha L/\lambda_D$ for $z_+ = 2, z_- = 1$ is higher than $z_+ = 1, z_- = 1$, in contrast to finite-ion size effects. These differences arise due to trends in $\dfrac{d\Psi}{dX}$; see Equation (30a) and Fig. 7(b).

The effect of γ_+/γ_- on $\alpha L/\lambda_D$ is summarized in Fig. 7(c) for $\gamma_+ c_0 = 3$, $z_+ = 1$ and $z_- = 1$. The dimensionless salt uptake $\alpha L/\lambda_D$ increases for decrease in γ_- since for $\Psi_D > 0$, the saturation concentration of anions is larger; see Equation (33). Therefore, a larger amount of salt can be taken up by the double layer.

Scaling analysis

We now develop scaling relations to better analyze the effect of the dielectric decrement. To estimate the location of extrema in $\mathbb{C}$ versus Ψ_D and their dependence on the values of z_+ and z_-, we invoke physical arguments. For $\Psi_D > 0$, negative ions will be attracted to the surface and the condition for a local maximum implies $c_- = \mathcal{O}\left(\frac{\varepsilon_s}{2\gamma_-}\right)$. In contrast, for $\Psi_D < 0$, the condition for a local maximum becomes $c_+ = \mathcal{O}\left(\frac{\varepsilon_s}{2\gamma_+}\right)$. Thus, assuming the $c_\pm$ follow the Boltzmann distribution, we get

$$\begin{aligned} z_- c_0 \exp(-z_+ \Psi_{D,\max}) &= \mathcal{O}\left(\frac{\varepsilon_s}{2\gamma_+}\right) \text{ for } \Psi_D \leq 0, \\ z_+ c_0 \exp(z_- \Psi_{D,\max}) &= \mathcal{O}\left(\frac{\varepsilon_s}{2\gamma_-}\right) \text{ for } \Psi_D \geq 0, \end{aligned} \tag{37}$$

or

$$\begin{aligned} -\Psi_{D,\max} &= \mathcal{O}\left(z_+^{-1} \ln\left(\frac{\varepsilon_s}{2 z_- \gamma_+ c_0}\right)\right) \text{ for } \Psi_D \leq 0, \\ \Psi_{D,\max} &= \mathcal{O}\left(z_-^{-1} \ln\left(\frac{\varepsilon_s}{2 z_+ \gamma_- c_0}\right)\right) \text{ for } \Psi_D \geq 0. \end{aligned} \tag{38}$$

We hypothesize that to predict a local minimum follows the same argument as before; see Equation (24). We summarize our results from the scaling analysis in Fig. 11. We find that both Equation (38) and (24) are in good agreement with the computed values.

In this section, we evaluated the influence of electrolyte valence on the dielectric decrement effect. Though we analyzed the case of a linear dielectric decrement, it is straightforward to extend this analysis to the case of non-linear dielectric decrement. We refer the readers to reference 32 for more details. Next, we analyze the effect electrolyte valence of ion-ion correlations on double layer properties.

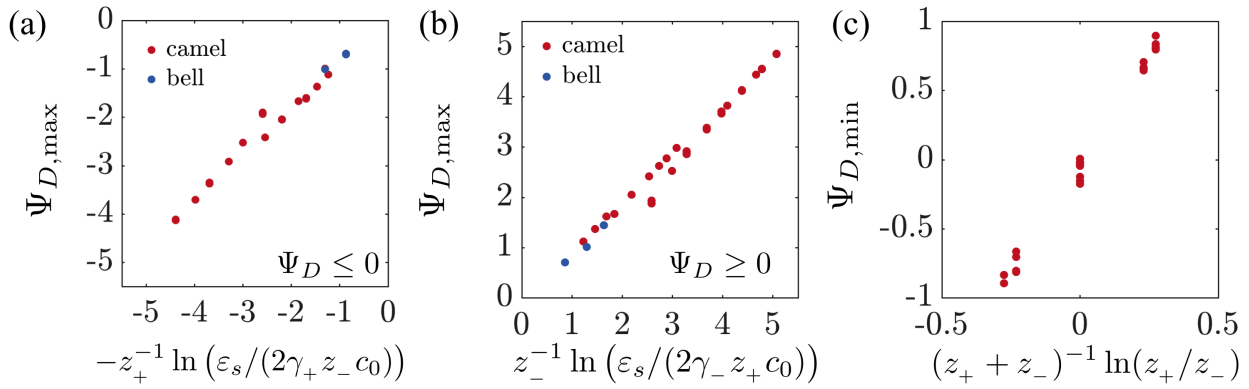

Figure 11: Scaling analysis of dielectric decrement effects. Comparison of computed $\Psi_{D,\max}$ with Equation (38) for (a) $\Psi_D < 0$ and (b) $\Psi_D > 0$. (c) Comparison of computed $\Psi_{D,\min}$ with Equation (24). The red points are cases with the camel shape *i.e.* two local maxima and one local minima, and the blue points are cases with the bell shape *i.e.* one local maximum. For computations, $0.25 \leq \gamma_+ c_0 \leq 3$, $1 \leq \gamma_+/\gamma_- \leq 4$, $1 \leq z_+ \leq 3$, and $1 \leq z_- \leq 3$. $\varepsilon_s = 80$ is assumed for all calculations.

Physical significance

We now present physical arguments to explain the significance of electrolyte valence on the dielectric decrement, which relates to the decrease in dielectric constant due to reduction in orientational polarizability. Simply put, a decrease in dielectric constant relates to reduction in the ability of the electrolyte to accumulate charge. The dielectric constant decreases with increase in ion concentration, and in this article we assume a linear decrement; see Equation (26). When the electrolyte comes in contact with a charged surface, due to electrostatic attraction, the concentration of counter ions increases closer to the surface. Consequently, the dielectric constant, and the ability to store charge, decrease closer to the surface. For a large potential drop across the double layer, these two effects are comparable and result in saturation of the counter ions near the surface; see Equation (33). It might appear that this effect is very similar to finite ion size where the concentration of counter ions also saturates, and thus equivalent expressions can be derived by replacing the maximum ion concentration $\frac{1}{a_-^3}$ with $\frac{\varepsilon_s}{2\gamma_-}$ and $\frac{1}{a_+^3}$ with $\frac{\varepsilon_s}{2\gamma_+}$. However, upon comparison of Equations (20) and (35), we note two differences, (i) a reduction by a factor of 2, and (ii) an apparent decrease in Ψ_D. The reduction by a factor of 2 occurs because the dielectric constant is reduced by a

factor of 2 at the surface; see Equation (33). On the other hand, the apparent decrease in Ψ_D occurs because when the dielectric decrement is included, the energy stored in electric field also varies with ion concentration. Therefore, to keep the double layer in equilibrium, the electric field energy negates the potential energy, leading to a smaller effective potential drop across the double layer.

The effect of asymmetry in electrolyte valence is non-trivial, as shown in Fig. 8(b) and Fig. 9(b). We observe that the effect of electric field energy dominates for small potential drops such that Q for $z_+ = 1, z_- = 1$ is lower than Q for $z_+ = 1, z_- = 3$, unlike Fig. 3(b). Furthermore, inclusion of valence asymmetry leads to asymmetry in capacitance values, see Fig. 9(b), similar to the case with finite ion size. Therefore, regardless of which effect (the finite ion size or the dielectric decrement) dominates, the inclusion of valence asymmetry leads to asymmetry in capacitance values. As noted before, the asymmetry in capacitance is valuable since capacitance influences the charge storage capacity and time scale of double layer formation. Therefore, for applications such as capacitive deionization,[3,46] it will be crucial to account for valence asymmetry since it significantly impacts the process variables.

In summary, dielectric decrement leads to the counter-ion saturation, the decrease in dielectric constant at the surface, and the decrease in the effective potential drop across the double layer due to variation in electric field energy with ion concentration. The effect of valence is non-trivial, especially for small Ψ_D, when the effect of variation in electric field energy is dominant. Furthermore, an asymmetry in electrolyte valence results in asymmetric double layer properties.

Ion-ion correlations

In this section, we consider the combined effect of ion-ion correlations and the steric effect. For simplicity, we do not consider the effect of the dielectric decrement and Stern layer in this section. For ion-ion correlations, we build on the work of Bazant, Storey and Kornyshev,[23,35] and we refer the readers to these references for the derivation of the modified Gauss law, which is given as

$$\varepsilon_0\varepsilon_s\left(l_c^2\frac{d^4\psi}{dx^4}-\frac{d^2\psi}{dx^2}\right)=z_+ec_+-z_-ec_-, \tag{39}$$

where l_c is the correlation length that quantifies the effect of ion-ion correlations. Equation (39) is to be solved with boundary conditions $\psi(0)=\psi_D$, $\left.\frac{d^3\psi}{dx^3}\right|_{x=0}=0$, and $\psi(\infty)=0$. We non-dimensionalize Equation (39) with $X=\frac{x}{\lambda_D}$, $n_+=\frac{c_+}{z_-c_0}$, $n_-=\frac{c_-}{z_+c_0}$, $L_c=\frac{l_c}{\lambda_D}$ to arrive at

$$L_c^2\frac{d^4\Psi}{dX^4}-\frac{d^2\Psi}{dX^2}=\frac{n_+-n_-}{z_++z_-}, \tag{40}$$

where $n_\pm$ are given by Equation (7). We numerically integrate Equation (40) to find $\Psi(X)$ and $n_\pm(X)$. From the numerical integration, we evaluate the dimensionless charge and salt uptake as

$$Q=\int_0^\infty\left(\frac{n_--n_+}{z_++z_-}\right)dX, \tag{41a}$$

$$\frac{\alpha L}{\lambda_D}=\int_0^\infty\left(\frac{z_-n_++z_+n_-}{z_++z_-}-1\right)dX. \tag{41b}$$

Lastly, we can also numerically evaluate the dimensionless capacitance as $\mathbb{C}=\left|\frac{dQ}{d\Psi_D}\right|$. We also note that analytical solutions of Equation (40) are only possible for $|\Psi_D|\ll 1$, and we refer the readers to reference 35 for more details.

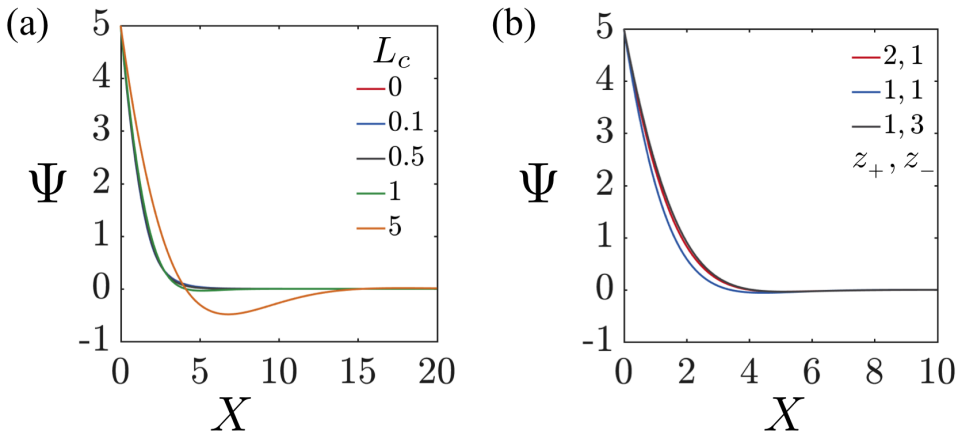

Figure 12: **Effect of asymmetry in electrolyte valence on ion-ion correlations**. Variation of Ψ with X as given by the solution of Equation (40) for $\Psi_D = 5$. (a) Effect of L_c with $a_+^3 c_0 = 0.2$, $a_+/a_- = 1$, $z_+ = 1$ and $z_- = 3$. (b) Effect of z_+ and z_- with $L_c = 1$, $a_+^3 c_0 = 0.2$ and $a_+/a_- = 1$.

Potential

We first the discuss the effect of $L_c = l_c \lambda_D^{-1}$ on the potential $\Psi(X)$. For $a_+^3 c_0 = 0.2, a_+/a_- = 1, z_+ = 1$ and $z_- = 3$, we find that for small values of L_c, *i.e* $L_c \leq 0.5$, the variations in $\Psi(X)$ are not significant. However, for larger values of L_c, we start to see oscillations in $\Psi(X)$, as previously described by Bazant and coworkers.[23,35]

Similar to finite-ion size and dielectric decrement effects, the effect of asymmetry in electrolyte valence is significant for ion-ion correlation effects. Fig. 12(b) shows the effect of change in z_+ and z_- for $L_c = 1$, $a_+^3 c_0 = 0.2$ and $a_+/a_- = 1$. We find that combination of cation and anion valence also influences the $\Psi(X)$ and the degree of oscillations. The parameters $a_+^3 c_0$ and a_+/a_- can also be varied. However, these effects have already been discussed in detail in the previous sections and we expect the qualitative trend to remain the same even with the inclusion of ion-ion correlations.

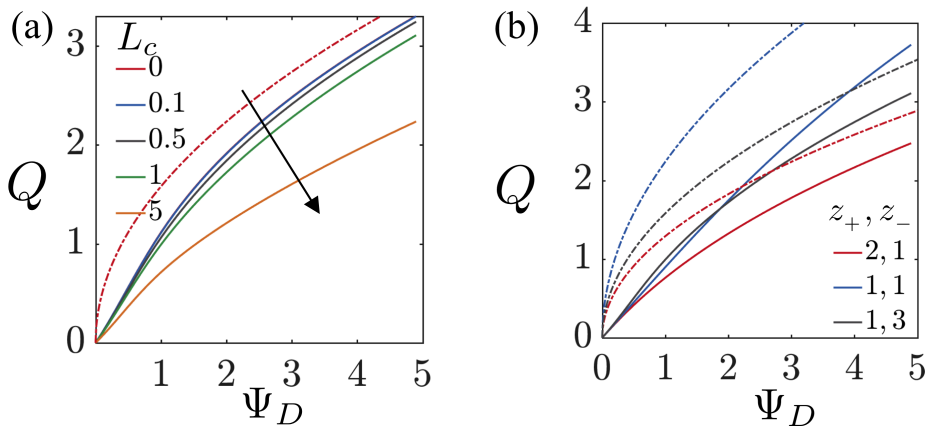

Figure 13: Effect of asymmetry in electrolyte valence on ion-ion correlations for $Q(\Psi_D)$, as given by the solution of Equations (40) and (41a), plotted here in solid lines. We also represent the approximate solution as given by Equation (20) for $L_c = 0$ with dotted lines. (a) Effect of L_c with $a_+^3 c_0 = 0.2$, $a_+/a_- = 1$, $z_+ = 1$ and $z_- = 3$. (b) Effect of z_+ and z_- with $L_c = 1$, $a_+^3 c_0 = 0.2$ and $a_+/a_- = 1$.

Charge accumulated

The oscillations in $\Psi(X)$ due to ion-ion correlations impact the charge accumulated inside the double layer. The effect of L_c on Q for $a_+^3 c_0 = 0.2$, $a_+/a_- = 1$, $z_+ = 1$ and $z_- = 3$ is provided in Fig. 13(a). We expect that oscillations in $\Psi(X)$ to be larger for larger value of L_c. Therefore, Q decreases with increase in the value of L_c. However, we emphasize that the shape of the curves are similar to the scenario without ion-ion correlations and for $L_c \leq 0.5$, Equation (20) can be used as a first-order approximation of Q, as shown in Fig. 13(a).

The effect of z_+ and z_- on $\Psi(X)$ for $L_c = 1$, $a_+^3 c_0 = 0.2$, $a_+/a_- = 1$ is provided in Fig. 13(b). The trends in Q are qualitatively similar to the results discussed in Fig. 3(b) and Equation (20). However, since $L_c = 1$, the magnitude of Q is slightly lower; see Fig. 13(a).

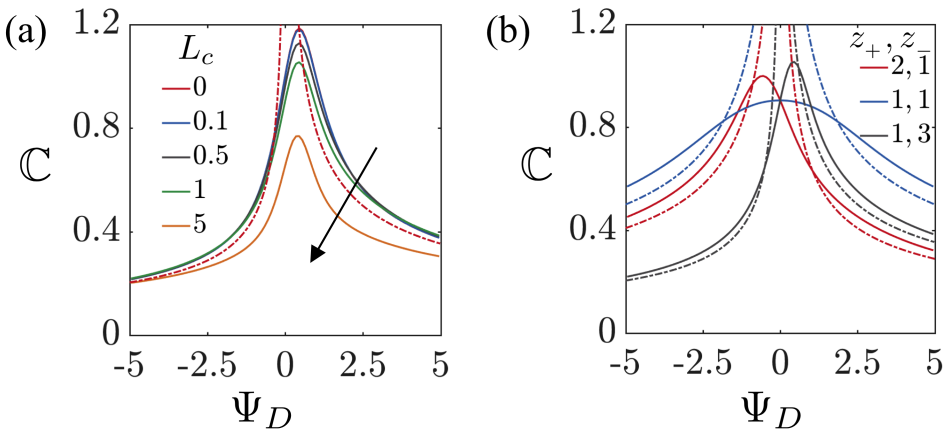

Figure 14: Effect of asymmetry in electrolyte valence on ion-ion correlations for $\mathbb{C}(\Psi_D)$, as given by the solution of Equations (40) and (41a), plotted here in solid lines. We also represent the approximate solution as given by Equation (21) for $L_c = 0$ with dotted lines. (a) Effect of L_c with $a_+^3 c_0 = 0.2$, $a_+/a_- = 1$, $z_+ = 1$ and $z_- = 3$. (b) Effect of z_+ and z_- with $L_c = 1$, $a_+^3 c_0 = 0.2$ and $a_+/a_- = 1$.

Capacitance

We now discuss the effect of ion-ion correlations on the capacitance $\mathbb{C}$. Since $\mathbb{C}$ measures the amount of charge per unit potential drop, we expect the ion-ion correlations to have a similar impact on $\mathbb{C}$ as it has on Q. Fig. 14(a) describes the variation of $\mathbb{C}$ for different L_c and $a_+^3 c_0 = 0.2$, $a_+/a_- = 1$, $z_+ = 1$ and $z_- = 3$. We note that since $a_+^3 c_0 = 0.2$, $\mathbb{C}$ versus Ψ_D is a bell shaped curve with the maximum at $\Psi_D > 0$, similar to Fig. 4(a). Upon increase in the value of L_c, the shape of the curve doesn't change. However, the values of $\mathbb{C}$ decrease with increase in Ψ_D, because an increase in L_c leads to fluctuations in charge density profiles, which in turn leads to a smaller amount of charge stored. We note that for $L_c \leq 0.5$, the change in $\mathbb{C}(\Psi_D)$ is not significant and we can use Equation (21) to approximate $\mathbb{C}(\Psi_D)$, especially for large $|\Psi_D|$, as shown.

As mentioned previously, L_c does not significantly influence the shape of $\mathbb{C}$ versus Ψ_D. Therefore, the effect of z_+ and z_- should be similar to the results reported in Fig. 4(b), which is indeed the case as shown in Fig. 14(b) where $\mathbb{C}$ values are calculated for different z_+ and z_- with $L_c = 1$, $a_+^3 c_0 = 0.2$ and $a_+/a_- = 1$. As expected, we find that the shape of $\mathbb{C}$

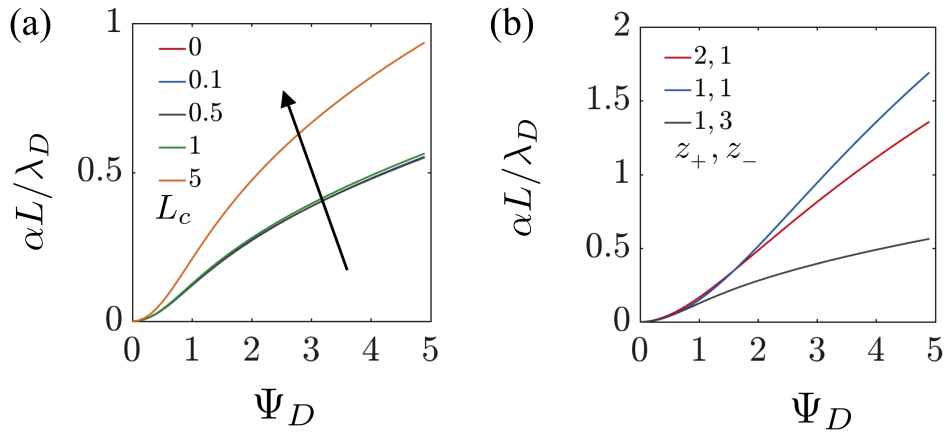

Figure 15: **Effect of asymmetry in electrolyte valence on ion-ion correlations**. Variation of $\alpha L/\lambda_D$ with Ψ_D as given by numerical integration of solution of Equation (40) and (41b). (a) Effect of L_c with $a_+^3 c_0 = 0.2$, $a_+/a_- = 1$, $z_+ = 1$ and $z_- = 3$. (b) Effect of z_+ and z_- with $L_c = 1$, $a_+^3 c_0 = 0.2$ and $a_+/a_- = 1$.

versus Ψ_D remains a bell shape. However, the position of a local maximum shifts due to the change in z_+ and z_-. For $z_+ = 1$ and $z_- = 1$, $\mathbb{C}$ versus Ψ_D is symmetric and has a maximum at $\Psi_D = 0$. However, for $z_+ = 2$ and $z_- = 1$, the maximum shifts to $\Psi_D < 0$, similar to the results shown in Fig. 4(b). We also show that we can approximate the capacitance $\mathbb{C}$ for large Ψ_D using Equation (21).

Salt uptake

Due to the oscillations in potential arising from ion-ion correlations, both charge Q and capacitance $\mathbb{C}$ decrease with increase in the correlation length L_c since a larger amount of repelled ions migrate inside the double layer. Therefore, these oscillations could result in an increase in the total amount of dimensionless salt uptake, which is in fact what we observe in Fig. 15(a) where $\alpha L/\lambda_D$ is measured for different L_c with $a_+^3 c_0 = 0.2$, $a_+/a_- = 1$, $z_+ = 1$ and $z_- = 3$. Here, we see the increase in $\alpha L/\lambda_D$ is relatively insignificant for $L_c \leq 0.5$. However, for larger values of L_c we find that the increase in $\alpha L/\lambda_D$ is quite significant.

We now discuss the effect of z_+ and z_- on $\alpha L/\lambda_D$ with $L_c = 1$, $a_+^3 c_0 = 0.2$ and $a_+ =$

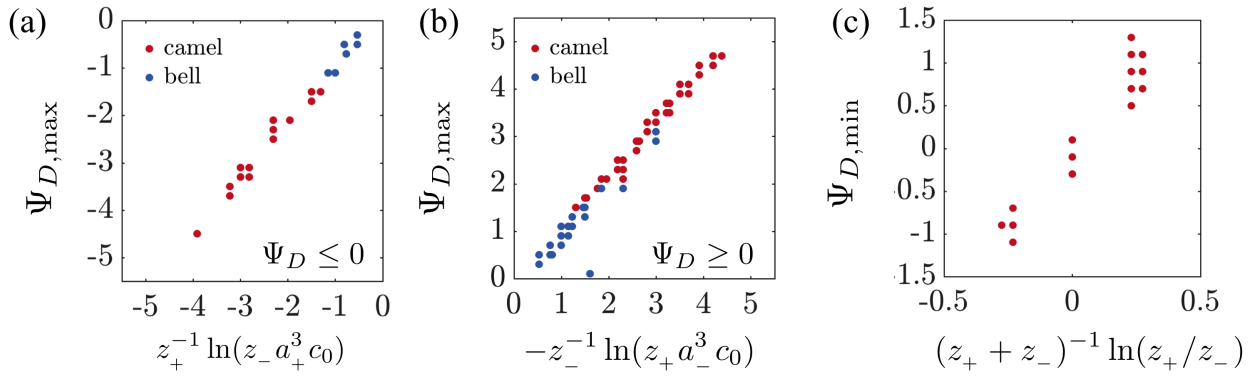

Figure 16: **Scaling analysis of ion-ion correlation effects**. Comparison of computed $\Psi_{D,\max}$ with Equation (23) for (a) $\Psi_D < 0$ and (b) $\Psi_D > 0$. (c) Comparison of computed $\Psi_{D,\min}$ with Equation (24). The red points are cases with the came shape *i.e.* two local maxima and one local minima, and the blue points are cases with the bell shape *i.e.* one local maximum. For computations, $0.02 \leq a_+^3 c_0 \leq 0.2$, $1 \leq a_+^3/a_-^3 \leq 4$, $1 \leq z_+ \leq 3$, $1 \leq z_- \leq 3$ and $0.1 \leq L_c \leq 5$.

$1/a_- = 1$, see Fig. 15(b). The trends of z_+ and z_- with the ion-ion correlations is the same as without finite-ion size effects; see Fig. 5(b). For instance, when we compare $z_+ = 1, z_- = 3$ with $z_+ = 1, z_- = 1$. Since $\Psi_D > 0$, Ψ_D at which ions saturate is lower for $z_+ = 1, z_- = 3$ than $z_+ = 1, z_- = 1$ and thus, $\alpha L/\lambda_D$ is lower for $z_+ = 1, z_- = 3$. In other words, the trends of $\alpha(\Psi_D)$ remain similar even though $\alpha L/\lambda_D$ is higher due to ion-ion correlations.

Scaling analysis

As mentioned above, the effect of ion-ion correlations typically do not significantly influence the shape of Q, $\mathbb{C}$ and $\alpha L/\lambda_D$ but does affect the magnitude of these properties. Therefore, we predict that $\Psi_{D,\max}$ and $\Psi_{D,\min}$ follow Equation (23) and (24). We summarize a comparison of predicted values using Equation (23) and (24), and computed values in Fig. 16, where our predictions are in good agreement with the computations. We note that though the location of $\Psi_{D,\max}$ and $\Psi_{D,\min}$ is similar to the scenarios without ion-ion correlations, the magnitude of Q and $\mathbb{C}$ are different upon inclusion of ion-ion correlations.

Physical significance

As noted before, the inclusion of ion-ion correlations leads to oscillations in charge density profiles. Therefore, the values of Q and $\mathbb{C}$ decrease with increase in correlation length since the repelled ions are present in the double layer at higher concentration. The effect of z_+ and z_- is similar to finite ion size and dielectric decrement, *i.e.* the asymmetry in valence leads to asymmetry in double layer properties. As shown in Fig. 14(b), even when ion-ion correlations are significant, the asymmetry in electrolyte valence breaks the symmetry of the capacitance, which underscores the need to incorporate the effect for more accurate predictions.

Summary and Outlook

In this article, we studied the effect of asymmetry in electrolyte valence on finite ion size, dielectric decrement and ion-ion correlation effects. For finite ion size, we considered the scenario with different cation and anion diameters. We analytically derived expressions for surface charge density $Q(\Psi_D)$, capacitance $\mathbb{C}(\Psi_D)$ and dimensionless salt $\alpha(\Psi_D)$, and numerically solved for the variation of the potential distribution $\Psi(X)$. These results have been discussed in Equation (12), (13) and (19). To the best of our knowledge, these are the most general expressions for diffuse-layer properties with steric effects. Wherever possible, we derived simplified expression for $Q(\Psi_D)$ and $\mathbb{C}(\Psi_D)$, and these results are provided in Equation (20) and (21). Furthermore, we developed scaling relations for local extrema such as $\Psi_{D,\text{max}}$ and $\Psi_{D,\text{min}}$ observed in the behavior of $\mathbb{C}$ versus Ψ_D, and these results are presented in Equation (23) and (24).

For the dielectric decrement, we considered the scenario of a linear dielectric decrement. We derived the fundamental equations that enable us to numerically solve for $\Psi(X)$, $Q(\Psi_D)$, $\mathbb{C}(\Psi_D)$ and $\alpha(\Psi_D)$ for non $z:z$ electrolytes. These results are presented in Equation (30).

We also present simplified expressions for $Q(\Psi_D)$ and $\mathbb{C}(\Psi_D)$ in Equations (35) and (36). The scaling relations for dielectric decrement results are presented in Equation (38) and (24).

Lastly, for ion-ion correlations, we numerically solve Equation (40) to obtain $\Psi(X)$, $Q(\Psi_D)$, $\mathbb{C}(\Psi_D)$ and $\alpha(\Psi_D)$. Here, we emphasize that Equations (20) and (21) provide a good starting approximation for small values of the correlation length L_c. We also show that scaling relations for finite-ion size effects, *i.e.* Equations (23) and (24), are applicable even after the inclusion of ion-ion correlations.

Our findings are important for mean field double layer theory, diffuse-charge dynamics and electrokinetics. We show that asymmetry in cation and anion valences play an important role in diffuse-layer properties and should be included in calculations of $Q(\Psi_D)$, $\mathbb{C}(\Psi_D)$, and $\alpha(\Psi_D)$. Going forward, we expect our results to be also useful in time-dependent problems. For instance, since z_+ and z_- influence $\alpha(\Psi_D)$, asymmetry in electrolyte valence will also influence the charging-discharging dynamics of the electrolyte between electrodes. Charging-discharging dynamics, which is relevant for the design of energy storage devices,[8,9] is especially important at large $|\Psi_D|$ where finite-ion size and dielectric decrement effects are pronounced, and valence asymmetry effects can be potentially exploited to control these effects. We also expect that our description of chemical potentials can be directly used to derive modified Nerst Plank equations in future studies. Moreover, the dimensionless salt uptake $\alpha(\Psi_D)$ could influence the adsorption quality and time scale for toxic heavy metal ion separations in capacitive deionization.[3,46]

We note that though we incorporated several modifications to the classical Poisson-Boltzmann model for valence asymmetric electrolytes, there are some limitations in our analysis and future work should focus on overcoming these limitations. For instance, we considered a simple hard-sphere model to include the steric effects and future work can focus on extending the

analysis of asymmetry in electrolyte valence on more accurate approaches to include steric effects.[25,49,50] Further, we assume a linear dielectric decrement model. Though the linear model works reasonably for electrolyte concentrations upto a few molars,[48] it is possible to extend our results to the scenario of non-linear decrement, and the future efforts should be directed in this direction.[32] Our treatment of many body interactions in ion-ion correlations is limited to the derivative of the potential and more sophisticated models could be considered in subsequent research.[51] Furthermore, a direct comparison between mean-field theory and sophisticated models such as density functional theory, Monte-Carlo simulations and molecular dynamics simulations,[49,52,53] will help test the validity of the mean-field results, and should be considered by researchers in the field. Lastly, we do not consider important effects such as specific forces[54] and hydration forces,[55,56] which have been a topic of recent interest, and should also be included in future studies.

Acknowledgement

We are thankful for support from the Andlinger Center for Energy and the Environment at Princeton University and the National Science Foundation (CBET - 1702693). The authors thank Pawel J. Zuk and Guang Chen for useful discussions. We also thank the anonymous referees for very helpful feedback that improved the paper.

References

(1) Dukhin, S. Non-equilibrium Electric Surface Phenomena. *Adv. Colloid Interface Sci.* **1993**, *44*, 1–134.

(2) Anderson, J. L. Colloid Transport by Interfacial Forces. *Annu. Rev. Fluid Mech.* **1989**, *21*, 61–99.

(3) Bazant, M. Z.; Thornton, K.; Ajdari, A. Diffuse-charge Dynamics in Electrochemical Systems. *Phys. Rev. E* **2004**, *70*, 021506.

(4) Anderson, J. L.; Keith Idol, W. Electroosmosis Through Pores with Nonuniformly Charged Walls. *Chem. Eng. Commun.* **1985**, *38*, 93–106.

(5) O'Brien, R. W.; White, L. R. Electrophoretic Mobility of a Spherical Colloidal Particle. *J. Chem. Soc., Faraday Trans. 2* **1978**, *74*, 1607–1626.

(6) Prieve, D.; Anderson, J.; Ebel, J.; Lowell, M. Motion of a Particle Generated by Chemical Gradients. Part 2. Electrolytes. *J. Fluid Mech.* **1984**, *148*, 247–269.

(7) Velegol, D.; Garg, A.; Guha, R.; Kar, A.; Kumar, M. Origins of Concentration Gradients for Diffusiophoresis. *Soft Matter* **2016**, *12*, 4686–4703.

(8) Simon, P.; Gogotsi, Y. Materials for Electrochemical Capacitors. *Nat. Mater.* **2008**, *7*, 845–854.

(9) Biesheuvel, P.; Bazant, M. Nonlinear Dynamics of Capacitive Charging and Desalination by Porous Electrodes. *Phys. Rev. E* **2010**, *81*, 031502.

(10) Presser, V.; Dennison, C. R.; Campos, J.; Knehr, K. W.; Kumbur, E. C.; Gogotsi, Y. The Electrochemical Flow Capacitor: A New Concept for Rapid Energy Storage and Recovery. *Adv. Energy Mater.* **2012**, *2*, 895–902.

(11) Gouy, M. Sur la Constitution de la Charge Électrique à la Surface d'un Électrolyte. *J. Phys. Theor. Appl.* **1910**, *9*, 457–468.

(12) Chapman, D. L. LI. A Contribution to the Theory of Electrocapillarity. *Philos. Mag.* **1913**, *25*, 475–481.

(13) Newman, J.; Thomas-Alyea, K. E. *Electrochemical Systems*; John Wiley & Sons, 2012.

(14) Bard, A. J.; Faulkner, L. R.; Leddy, J.; Zoski, C. G. *Electrochemical Methods: Fundamentals and Applications*; Wiley, 1980; Vol. 2.

(15) Hunter, R. J. *Foundations of Colloid Science*, 2nd ed.; Oxford University Press, 2001.

(16) Delgado, Á. V.; González-Caballero, F.; Hunter, R.; Koopal, L.; Lyklema, J. Measurement and Interpretation of Electrokinetic Phenomena. *J. Colloid Interface Sci.* **2007**, *309*, 194–224.

(17) Stern, O. Zur Theorie der Elektrolytischen Doppelschicht. *Ber. Bunsenges. Phys. Chem.* **1924**, *30*, 508–516.

(18) Bikerman, J. Structure and Capacity of Electrical Double Layer. *Lond. Edinb. Dubl. Phil. Mag.* **1942**, *33*, 384–397.

(19) Freise, V. Zur Theorie Der Diffusen Doppelschicht. *Ber. Bunsenges. Phys. Chem.* **1952**, *56*, 822–827.

(20) Kornyshev, A. A. Double-layer in Ionic Liquids: Paradigm change? 2007.

(21) Kilic, M. S.; Bazant, M. Z.; Ajdari, A. Steric Effects in the Dynamics of Electrolytes at Large Applied Voltages. I. Double-layer Charging. *Phys. Rev. E* **2007**, *75*, 021502.

(22) Ben-Yaakov, D.; Andelman, D.; Harries, D.; Podgornik, R. Beyond Standard Poisson–Boltzmann Theory: Ion-specific Interactions in Aqueous Solutions. *J. Phys.: Condens. Matterr* **2009**, *21*, 424106.

(23) Bazant, M. Z.; Storey, B. D.; Kornyshev, A. A. Double Layer in Ionic Liquids: Overscreening versus Crowding. *Phys. Rev. Lett.* **2011**, *106*, 046102.

(24) Fedorov, M. V.; Kornyshev, A. A. Towards Understanding the Structure and Capacitance of Electrical Double Layer in Ionic Liquids. *Electrochim. Acta* **2008**, *53*, 6835–6840.

(25) Bazant, M. Z.; Kilic, M. S.; Storey, B. D.; Ajdari, A. Towards an Understanding of Induced-charge Electrokinetics at Large Applied Voltages in Concentrated Solutions. *Adv. Colloid Interface Sci.* **2009**, *152*, 48–88.

(26) Sparnaay, M. J. *The Electrical Double Layer*; Pergamon, 1972; Vol. 4.

(27) Borukhov, I.; Andelman, D.; Orland, H. Adsorption of Large Ions from an Electrolyte Solution: A Modified Poisson–Boltzmann Equation. *Electrochim. Acta* **2000**, *46*, 221–229.

(28) Kilic, M. S.; Bazant, M. Z.; Ajdari, A. Steric Effects in the Dynamics of Electrolytes at Large Applied Voltages. II. Modified Poisson-Nernst-Planck equations. *Phys. Rev. E* **2007**, *75*, 021503.

(29) Han, Y.; Huang, S.; Yan, T. A Mean-field Theory on the Differential Capacitance of Asymmetric Ionic Liquid Electrolytes. *J. Phys.: Condens. Matter* **2014**, *26*, 284103.

(30) Biesheuvel, P. M. Volume Exclusion Effects in the Ground-state Dominance Approximation for Polyelectrolyte Adsorption on Charged Interfaces. *Eur. Phys. J. E: Soft Matter Biol. Phys.* **2005**, *16*, 353–359.

(31) Hatlo, M. M.; Van Roij, R.; Lue, L. The Electric Double Layer at High Surface Potentials: The Influence of Excess Ion Polarizability. *EPL* **2012**, *97*, 28010.

(32) Nakayama, Y.; Andelman, D. Differential Capacitance of the Electric Double Layer: The Interplay between Ion Finite Size and Dielectric Decrement. *J. Chem. Phys.* **2015**, *142*, 044706.

(33) Ben-Yaakov, D.; Andelman, D.; Harries, D.; Podgornik, R. Ions in Mixed Dielectric Solvents: Density Profiles and Osmotic Pressure between Charged Interfaces. *J. Phys. Chem. B* **2009**, *113*, 6001–6011.

(34) Ben-Yaakov, D.; Andelman, D.; Podgornik, R. Dielectric Fecrement as a Source of Ion-specific Effects. *J. Chem. Phys.* **2011**, *134*, 074705.

(35) Storey, B. D.; Bazant, M. Z. Effects of Electrostatic Correlations on Electrokinetic Phenomena. *Phys. Rev. E* **2012**, *86*, 056303.

(36) Grahame, D. C. Diffuse Double Layer Theory for Electrolytes of Unsymmetrical Valence Types. *J. Chem. Phys.* **1953**, *21*, 1054–1060.

(37) Levine, S.; Jones, J. Interaction of Two Parallel Colloidal Plates in an Electrolyte Mixture of Univalent and Divalent Ions. *Colloid Polym. Sci.* **1969**, *230*, 306–317.

(38) Lyklema, J. *Fundamamentals of Interface and Colloid Science*; Academic Press, 1995; Vol. 2.

(39) Joshi, K.; Parsons, R. The Diffuse Double Layer in Mixed Electrolytes. *Electrochim. Acta* **1961**, *4*, 129–140.

(40) Levie, R. D. Notes on Gouy diffuse-layer Theory. *J. Electroanal. Chem. Interfacial Electrochem.* **1990**, *278*, 17–24.

(41) *Fundamamentals of Interface and Colloid Science*.

(42) Zhao, R.; Van Soestbergen, M.; Rijnaarts, H.; Van der Wal, A.; Bazant, M.; Biesheuvel, P. Time-dependent Ion Selectivity in Capacitive Charging of Porous Electrodes. *J. Colloid Interface Sci.* **2012**, *384*, 38–44.

(43) Campos, J. W.; Beidaghi, M.; Hatzell, K. B.; Dennison, C. R.; Musci, B.; Presser, V.; Kumbur, E. C.; Gogotsi, Y. Investigation of Carbon Materials for Use as a Flowable Electrode in Electrochemical Flow Capacitors. *Electrochim. Acta* **2013**, *98*, 123–130.

(44) Gao, Y.; Qin, Z.; Guan, L.; Wang, X.; Chen, G. Z. Organoaqueous Calcium Chloride Electrolytes for Capacitive Charge Storage in Carbon Nanotubes at Sub-Zero-Temperatures. *Chemi. Comm.* **2015**, *51*, 10819–10822.

(45) Wang, H.; Pilon, L. Physical Interpretation of Cyclic Voltammetry for Measuring Electric Double Layer Capacitances. *Electrochim. Acta* **2012**, *64*, 130–139.

(46) Chu, K. T.; Bazant, M. Z. Nonlinear Electrochemical Relaxation around Conductors. *Phys. Rev. E* **2006**, *74*, 011501.

(47) Chen, Z.; Singh, R. K. General Solution for Poisson–Boltzmann Equation in Semi-infinite Planar Symmetry. *J. Colloid Interface Sci.* **2002**, *245*, 301–306.

(48) Hasted, J.; Ritson, D.; Collie, C. Dielectric Properties of Aqueous Ionic Solutions. Parts I and II. *J. Chem. Phys.* **1948**, *16*, 1–21.

(49) Giera, B.; Henson, N.; Kober, E. M.; Shell, M. S.; Squires, T. M. Electric Double-layer Structure in Primitive Model Electrolytes: Comparing Molecular Dynamics with Local-density Approximations. *Langmuir* **2015**, *31*, 3553–3562.

(50) Giera, B.; Henson, N.; Kober, E. M.; Squires, T. M.; Shell, M. S. Model-free Test of Local-density Mean-field Behavior in Electric Double Layers. *Phys. Rev. E* **2013**, *88*, 011301.

(51) Li, Z.; Wu, J. Density-functional Theory for the Structures and Thermodynamic Properties of Highly Asymmetric Electrolyte and Neutral Component Mixtures. *Phys. Rev. E* **2004**, *70*, 031109.

(52) Henderson, D.; Lamperski, S.; Jin, Z.; Wu, J. Density Functional Study of the Electric Double Layer Formed by a High Density Electrolyte. *The Journal of Physical Chemistry B* **2011**, *115*, 12911–12914.

(53) Lamperski, S.; Outhwaite, C. W.; Bhuiyan, L. B. The Electric Double-Layer Differential Capacitance at and Near Zero Surface Charge for a Restricted Primitive Model Electrolyte. *The Journal of Physical Chemistry B* **2009**, *113*, 8925–8929.

(54) Goodwin, Z. A.; Feng, G.; Kornyshev, A. A. Mean-field Theory of Electrical Double Layer in Ionic Liquids with Account of Short-range Correlations. *Electrochim. Acta* **2017**, *225*, 190–197.

(55) Bohinc, K.; Shrestha, A.; Brumen, M.; May, S. Poisson-Helmholtz-Boltzmann Model of the Electric Double Layer: Analysis of Monovalent Ionic Mixtures. *Phys. Rev. E* **2012**, *85*, 031130.

(56) Brown, M. A.; Bossa, G. V.; May, S. Emergence of a Stern layer from the Incorporation of Hydration Interactions into the Gouy–Chapman Model of the Electrical Double Layer. *Langmuir* **2015**, *31*, 11477–11483.

For Table of Contents Use Only